Submitted to Canadian Journal of Soil Science

Influence of landscape on the apportionment of Ca nutrition in a Boreal Shield forest of Saskatchewan (Canada) using $^{87}Sr/^{86}Sr$ as a tracer

Nicolas Bélanger[1*] and Chris Holmden[2]

[1]UER Sciences et technologies, Université du Québec à Montréal, 100 Sherbrooke Ouest, Montréal, Québec, Canada, H2X 3P2.

[2]Saskatchewan Isotope Laboratory, Department of Geological Sciences, University of Saskatchewan, 114 Science Place, Saskatoon, Saskatchewan, Canada, S7N 5E2.

*corresponding author - email: belanger.nicolas@teluq.uqam.ca; phone: (514) 987-3000 ext. 0900.

ABSTRACT

A $^{87}Sr/^{86}Sr$ tracer technique was used to apportion the supply of calcium (Ca) between atmospheric deposition and soil mineral weathering in a pristine Boreal Shield forest of northern Saskatchewan. To assess the impact of landscape variability on soil mineral weathering $^{87}Sr/^{86}Sr$ ratios, the watershed was divided into six study plots at low, middle, and high elevations along two toposequences—one consisting of mixed woods and the other consisting of black spruce. Apportionment analysis shows that none of the trees in the study plots depend entirely on soil mineral weathering as a source of Ca. Calcium pools in trees are shifted towards the atmospheric end-member (31–98%), probably because of the low soil mineral weathering fluxes combined with relatively high atmospheric deposition fluxes. These results need to be considered as the consequence of buildup and recycling of atmospherically derived Ca in the soil-vegetation system rather than the direct and large use of current atmospheric Ca inputs by the trees on an annualized basis. We also find that the trees in the high elevation plots contain more Ca from atmospheric sources (84–98%) than trees in middle (31-86%) and low (37-82%) elevation plots. Two mechanisms are proposed to explain these results. First, if each plot is assumed to receive a constant supply of atmospherically derived Ca, then hillslope changes in soil mineral weathering rates are required to explain the changing proportions of atmospherically derived Ca cycling internally within each plot. Second, trees on hilltops may capture more dry aerosols than trees that are more shielded from atmospheric circulation in the valleys. Our work supports previous Ca cycling models in other forested ecosystems suggesting that much of the Ca requirement in trees is met *via* the flux from the atmosphere, but adds knowledge in regards to the role of topographical effects and forest canopy height as local factors that can influence the balance of Ca captured from atmospheric sources and released from soil mineral weathering sources.

Keywords: Boreal forest; calcium cycling; atmospheric deposition; soil mineral weathering; strontium isotopes; $^{87}Sr/^{86}Sr$; calcium to strontium ratios; Sr/Ca; forest floor; tree calcium pools.

RÉSUMÉ

Une technique de traçage avec le ratio $^{87}Sr/^{86}Sr$ a été utilisée pour déterminer les contributions des dépôts atmosphériques et de l'altération des minéraux dans les sols quant aux réserves de calcium (Ca) dans une forêt vierge du bouclier boréal du nord de la Saskatchewan. Pour évaluer l'impact de la topographie sur les ratios $^{87}Sr/^{86}Sr$ de l'altération des sols, le bassin versant a été divisé en six parcelles, à partir de l'interfluve jusqu'au milieu et au bas de pente, le long de deux toposéquences, l'une dominée par l'épinette noire et l'autre représentant une forêt mélangée. L'analyse de répartition révèle qu'aucun des arbres étudiés ne dépend entièrement sur l'altération des minéraux dans les sols comme source de Ca. Les réserves de Ca dans les arbres tendent vers les dépôts atmosphériques (31 à 98%), probablement à cause des faibles taux d'altération des minéraux dans les sols en concomitance avec des flux atmosphériques relativement élevés. Les résultats doivent être interprétés comme la conséquence d'une accumulation et d'un recyclage du Ca atmosphérique dans le système plante-sol plutôt qu'une importante utilisation directe des apports atmosphériques actuels de Ca par les arbres sur une base annuelle. Les résultats révèlent aussi que les arbres en haut de versant contiennent davantage de Ca atmosphérique (84 à 98%) que les arbres poussant sur les milieux (31 à 86%) ou les bas (37 à 82%) de pentes. On propose deux mécanismes pour expliquer ces résultats. Premièrement, si l'on présume que chaque parcelle reçoit la même quantité de Ca via l'atmosphère, des changements dans les taux d'altération des sols sont requis pour expliquer les variations des apports de Ca atmosphérique dans chacune des parcelles. Deuxièmement, les arbres dans les hauts de versants filtrent davantage de particules sèches que dans les vallées qui dissimulent les arbres de la circulation atmosphérique. Nos travaux supportent quelques modèles sur le cycle du Ca dans d'autres écosystèmes forestiers qui suggèrent que les exigences en Ca des arbres sont en grande partie comblées par les flux atmosphériques, mais nous ajoutons des connaissances quant aux effets de la topographie et de la hauteur de la canopée des arbres sur le cycle du Ca.

Mots-clés: Forêt boréale; cycle du calcium; dépôts atmosphériques; alteration des minéraux dans les sols; isotopes de strontium; $^{87}Sr/^{86}Sr$; ratios calcium : strontium; Sr/Ca; humus forestier, réserves de calcium dans les arbres.

The boreal forest biome is the largest on earth. It also ranks as one of the most ecologically sensitive because of its long cold winters, short summers, and coarsely textured, base-poor, and weakly buffered soils, which slowly release base cations such as calcium (Ca) from mineral weathering (Kirkwood and Nesbitt 1991). Calcium is an essential plant nutrient. If forests are to prosper in this harsh environment, they must rely heavily on stores of Ca retained on ion exchange sites in soils, built up over centuries, and perhaps even millennia. These Ca stores are vulnerable to anthropogenic disturbances. During the past 50 years, increased air pollution with a concomitant increase in rain acidity has favored increased base cation exports in poorly buffered forests to a point that base cation availability may become as limiting to forest growth as nitrogen (Likens et al. 1996; Watmough et al. 2005). In addition, the transition to more intensive forest management practices (e.g. clearcutting as opposed to partial cutting or whole-tree harvesting as opposed to stem-only) may have exacerbated this export in areas where the boreal forest is being extensively logged (Olsson et al. 1996; Arocena 2000; Paré et al. 2002; Thiffault et al. 2006).

Although consensus is building that forests are highly dependent on recycled sources of Ca for their nutritional needs, only two inputs contribute significantly to the forest Ca cycle—atmospheric deposition and soil mineral weathering. Over the past couple of decades, studies have shown that these inputs may be distinguished using the isotopes of Sr as a proxy for Ca (see Table 1 for a list of references). The amount of ^{87}Sr varies in terrestrial materials due to the slow radioactive decay of ^{87}Rb. This enables $^{87}Sr/^{86}Sr$ to be used as a tracer of Sr sources in natural systems. If $^{87}Sr/^{86}Sr$ in atmospheric deposition differs from soil mineral weathering, then the two sources will become mixed in trees through uptake of Sr (which closely follows Ca) by fine roots

and its return to the forest floor through litterfall. Knowing the $^{87}Sr/^{86}Sr$ and Sr/Ca ratios of the atmospheric and soil mineral weathering end-members, and the mixed $^{87}Sr/^{86}Sr$ ratios in the trees, enables the fractions of Ca contributed by atmospheric deposition and soil mineral weathering to be deduced from isotope mass balance considerations (e.g., Capo et al. 1998). Forests on several continents spanning boreal, temperate, and tropical environments have been subjected to this analysis over the years, and the findings have contributed to a shift away from the traditional position that soil mineral weathering is the sole source of base cations in plant available pools, to one that recognizes the importance of atmospheric inputs (Table 1). In this paper, we apply the $^{87}Sr/^{86}Sr$ apportionment technique to the Ca cycle of a Boreal Shield forest for the first time. In the Boreal forest, fine root growth is positively and exponentially correlated to soil temperature (Tryon and Chapin 1983) and the warmer surface soil promotes organic matter turnover and nutrient availability (Flanagan and Van Cleve 1983). Therefore, we suspect that tree fine roots in Boreal Shield systems penetrate less deeply into the mineral soil (Strong and La Roi 1983; Finer et al. 1997; Steele et al. 1997) and that contribution of soil mineral weathering to Ca pools in trees is therefore reduced. The cooler the soils, the more decoupling there should be between fine roots and mineral soil to satisfy Ca demand for optimum growth. One of the motivations driving this work was to uncover the extent to which these climatic conditions control the level of atmospherically derived Ca in the uppermost soil layers and vegetation.

For the apportionment technique to work, atmospheric deposition and soil mineral weathering end-members must have contrasting $^{87}Sr/^{86}Sr$ ratios, and Sr and Ca cycling must be conservative. Confidence in the results also depends on the end-members being uniform in time and space and well mixed in the vegetation. To satisfy these criteria, many studies sought field sites in coastal regions where the $^{87}Sr/^{86}Sr$ signature of atmospheric deposition is dominated by sea spray (e.g., Vitousek et al. 1999; Kennedy et al. 2002). Sites were also chosen whose soil parent material exhibited simple mineralogy and texture, such as volcanic rocks or monomineralic plutonic rocks, in order to be certain that the $^{87}Sr/^{86}Sr$ signature of soil mineral weathering would

be uniform and independent of mineral weathering susceptibility (e.g., Kennedy et al. 1998; Vitousek et al. 1999). Vast areas of the world's Boreal Shield forests, however, grow far inland from the oceans, on soils developed from polymineralic parent materials, thus, considerably complicating the assessment of $^{87}Sr/^{86}Sr$ in precipitation and, in particular, soil mineral weathering. The study site near La Ronge is underlain by a 1.85 billion-year-old granite pluton, but the soil parent material is a glacial till, formed by subglacial erosion of the granite. The till was subsequently reworked in the near shore setting of a large proglacial lake (Agassiz), leaving behind a landscape characterized by coarser grained tills on hilltops and shallow clayey lacustrine deposits overlying tills in valleys. To address the extent to which topographically controlled changes in soil texture and mineralogy might influence $^{87}Sr/^{86}Sr$ weathering signatures, the study area was partitioned into plots, along two hillside toposequences at right angles to the stream. The $^{87}Sr/^{86}Sr$ ratio of the soil mineral weathering end-member is assessed individually for each plot using nitric acid leaches of mineral soils (lower B or BC horizons) to represent the release of Sr and Ca from natural mineral weathering (Nezat et al. 2007; 2008). These data, along with (1) field measurements of $^{87}Sr/^{86}Sr$ ratios in precipitation, soil solutions, stream water, and groundwater, and (2) estimates of the size of the above and below ground Ca pools and soil cation exchange capacities, enables us to completely characterize the $^{87}Sr/^{86}Sr$ variability of the study site. In turn, this enables us to conduct a thorough evaluation of the impact of landscape variability on the apportioning of Ca from atmospheric deposition and soil mineral weathering.

MATERIAL AND METHODS

Site Description

A 68 ha first-order forested watershed of the Churchill River Upland ecoregion, located along the southern edge of the Precambrian Shield in north-central Saskatchewan was selected for study in 2005. The watershed is located 40 km north of the town of La Ronge (55° 20' N, 105° 5'

W), approximately 400 km north of Saskatoon (Fig. 1). Mean annual air temperature and precipitation in La Ronge are respectively –0.1ºC and 484 mm (with 30% falling as snow). Two toposequences were selected for the study. Toposequence 1 varies from 393 m to 373 m asl (10 m high) and is 34 m long, whereas toposequence 2 is slightly longer at 35 m but varies in elevation from 392 m to 374 m asl (8 m high). Toposequence 2 is situated about 40 m upstream of toposequence 1. Toposequence 1 is dominated by mixed woods (trembling aspen [*Populus tremuloides* Michx.], black spruce [*Picea mariana* (Mill.) Bsp.] and jack pine [*Pinus banksiana* Lamb.]) from top to bottom, whereas toposequence 2 is composed of pure black spruce with feathermoss growing as the understorey. Some large white spruce (*Picea glauca* (Moench) Voss) and balsam poplar (*Populus balsamifera* L.) trees are also found towards the valley floor. The main cohort of trees is about 85 years of age, whereas the larger white spruce and balsam poplar trees are from an older cohort of 100 years. Both toposequences are composed of three 75 m^2 circular plots, i.e., at the highest elevation, at mid-elevation, and in the riparian area (≤3m away from the stream channel). The high elevation plots on toposequences 1 and 2 are respectively at 393 m and 391 m asl, the mid elevation plots are at 384 m and 382 m, and the low elevation plots (or riparian plots) are at 373 m and 374.

The mixed wood forest soils of toposequence 1 are relatively coarse grained, warm and drier in the mid- and high elevation plots, with jack pine growing on the driest sites. Soils of toposequence 2 are generally wetter and cooler. General soil physical and chemical properties are presented in Table 2. The soils are ultimately derived from granitic bedrock of the Glennie domain (~1.85 billion years old; Ansdell et al. 2005), which crops out at the top of the watershed. Mixed woods grow on sandy loam soils that developed as Eluviated Dystric Brunisols (Soil Classification Working Group 1998). The soils at mid-elevation are usually silty loam and developed as Brunisolic Gray Luvisols. The soils at the bottom are generally Orthic Gleysols and occasionally Humic Gleysols and are silty clay. The divergence in soil properties from top to bottom along each toposequence reflects reworking of glacial till in the post-glacial lacustrine

environment of glacial lake Agassiz. The study site is close to the western limit of its influence (Ojakangas and Matsch 1982). Shallow waters penetrated the watershed studied here, causing suspension, sorting, and ultimately the transport of fine sediments from shallow waters overlying the hilltops into deeper waters overlying the submerged valleys. Pedologists refer to this common feature of the landscape as the Jan Lake Complex (Acton et al. 1983). During the lacustrine phase, mixing with tills derived from other types of bedrock, like the felsic schists that crop out in the region [containing quartz, K-feldspar, biotite, muscovite and traces of calcite; Forsythe and Coates (1971)], may have occurred.

Sampling and Analytical Methods

Soil and Soil Solution

Within each plot, the forest floor was collected by cutting around a 20 cm × 20 cm template. The slash, litter layer, moss cover, and large roots were removed, leaving only the F and H layers and the fine roots (dead or living) in the sample. The mineral soil was sampled by diagnostic horizons up to the BC/C horizon, but the discontinuous Ae horizon of the Eluviated Brunisols was not sampled. Forest floor bulk density was obtained by measuring its depth and oven-dried mass at 65˚C. Bulk density of upper mineral soil was also assessed on oven-dried samples collected at 0-20 cm and 20-40 cm increments using a specifically designed corer.

In each plot, zero-tension lysimeters were installed at the transition between the forest floor and mineral soil (~10 cm) using the same procedures as described in MacDonald et al. (2007). In the high and mid-elevation plots, lysimeters were also installed in the mineral soil at a total depth (including forest floor) of approximately 35 cm. This corresponds to the bottom of the upper B horizon. Two porous cup tension lysimeters (Soil Moisture Equipment, Santa Barbara, CA) were installed at total depths of about 22 cm and 35 cm in the riparian plots due to the difficulties of installing zero-tension systems for soil pits that are affected by a shallow water

202 table. PVC piezometers with a 30 cm long micro-screen at the bottom were also installed in these
203 riparian plots at depths of 1.4 and 1.8 m to sample/monitor shallow groundwater. The soil
204 solution/groundwater samples were collected bi-monthly in 2005 (May to October).
205
206 ## *Vegetation*
207 Foliage and stemwood samples were collected in and around each plot before leaf
208 senescence from dominant or co-dominant black spruce, trembling aspen and jack pine. Each
209 sampled tree is identified by plot in Table 4. Foliage exposed to direct sunlight and located in the
210 upper half of the canopy was targeted with a shotgun. Stem wood was sampled at diameter at
211 breast height (1.3 m) with a 4.1 mm-diameter Haglöf® increment borer. Tree age was determined
212 on sanded tree cores using a boom stand binocular stereoscopic microscope. To facilitate aging of
213 trembling aspen, disks from two dominants or co-dominants per plot were collected by felling the
214 trees at 5 cm from the ground. In each plot, only diameter at breast height (DBH) at 1.3 m of the
215 trees with a stem diameter > 6 cm was noted in the field.
216 Allometric equations developed by Lambert et al. (2005) were used to estimate the
217 aboveground biomass density (organic dry mass per unit area) in each plot. Stem, bark, branches
218 and canopy biomass were assessed individually and by species using the DBH data as input.
219 Average Ca content for the various tree components was also calculated by species as Ca
220 concentration in component x × dry mass per m^2 of component x (i.e. wood, bark, branches and
221 foliage). Total aboveground Ca content in each plot was estimated as the sum of the Ca content in
222 stemwood, stem bark, foliage and branches. Calcium content in roots was not accounted for in
223 this study. Calcium concentrations used for the calculations are those in Table 3. As can be seen,
224 these are similar to Ca concentrations measured in wood and foliage at the study site.
225
226 ## *Atmospheric Deposition*

Rainwater was collected bi-monthly throughout the growing season using an automated and chemically clean wet-only deposition collector (Ecotech Model 200, Blackburn, Australia). The collector was installed on top of a 15 m high aircraft hangar that is used by the forest fire fighting crew just north of the town of La Ronge. Bulk deposition was also collected bi-monthly from polyethylene funnel collectors (diameter of 17.5 cm) that were installed at a height of 1.5 m in forest gaps inside the watershed. Collecting bottles were buried in the ground to prevent evaporation. In addition, snow samples were collected from Lac La Ronge (55° 06' N; 105° 16' W) and Nemeiben Lake (55° 17' N; 105° 13' W) in March 2005. Snow samples did not include the entire winter's snowfall accumulation and therefore the samples probably reflect the integrated atmospheric signal for the latter part of the winter season.

Soil Chemistry and Mineralogy

The elemental compositions of the lower B (or BC) horizons and granite bedrock were determined on 32-mm-diameter fused beads prepared from a 1:5 soil – lithium tetraborate mixture using an automated X-ray fluorescence spectrometer system (Philips PW2440 4kW) with a Rhodium 60 kV end window X-ray tube. The powders produced for X-ray fluorescence analysis were also mounted as non-oriented slides and analyzed by X-ray diffraction on a diffractometer (Rigaku RU-200) with a Fe-Kα radiation filtered by a graphite monochromator at 40 kV and 160 mA. A thin section of the granite was also prepared for the *in situ* measurement of the major elements in selected minerals using a JEOL 8600 Superprobe. Elemental analysis results were used to assign elements to their respective minerals using the UPPSALA norms for soils (Sverdrup and Warfvinge 1992) and CIPW norms for the granite. The UPPSALA model is a normative back-calculation model for reconstructing empirical soil mineralogy from total digestion analysis and is based on assumptions of the stoichiometric composition of the minerals in soils of granitic origin (i.e., Swedish Precambrian Shield). The minerals have been grouped

into assemblies of minerals with similar composition and dissolution rates. For example, chlorite is composed of trioctahedral chlorite, primary illite, trioctahedral vermiculite of primary type, and biotite, whereas epidote includes all epidotes and pyroxenes. X-ray diffraction results were used to validate the output from the UPPSALA and CIPW norms.

Soil Mineral Weathering

Because apatite is potentially a large contributor of Ca to trees in forests supported by relatively young soils (14 ka or less) derived from igneous and silicate-dominated metamorphic rocks, Nezat et al. (2007) developed a sequential extraction method that would isolate apatite so that its distribution in the profile and its exposure to soil solutions could be better understood. They separated individual silicate minerals from a parent material developed from granite, characterized the composition of each mineral, and subjected synthetic mixtures of these minerals to various sequential extraction treatments to determine which minerals dissolved at each step. The influence of acid type, strength, and temperature on the isolation of apatite dissolution was also tested. The method was finally tested against soils from the Hubbard Brook Experimental Forest where the mineralogy has been extensively studied. The data for granitic soils suggest that leaching with 1 N HNO_3 acid at 20°C for 20 h, at a soil:solution ratio of 10, almost entirely dissolves apatite. Even apatite found in rock fragments and, thus, surrounded by silicate minerals, was found to have dissolved from the acid attack if located along grain boundaries or mineral fractures. Small amounts of hornblende and biotite (or chlorite or vermiculite) were also attacked during this leach. At 200°C, the minerals that are dominantly dissolved by the 1 N HNO_3 solution at the same soil:solution ratio are biotite and chlorite. Although most of the apatite was removed during the lower temperature leach, the remainder (armored by biotite and chlorite) is dissolved in the high temperature leach. The left over silicate minerals, such as plagioclase and alkali feldspars, are dissolved in concentrated HF–HNO_3-HCl solutions, as well as any apatite

277 inclusions that remain. Importantly, Nezat et al. found that weaker extracts (e.g. 0.01 and 0.1 N
278 HNO_3) failed to dissolve apatite. Therefore, weak acid extractions are probably only appropriate
279 for soils containing calcite (e.g. Drouet et al. 2005). In another study, Nezat et al. (2008) tested
280 their method on C horizons developed on a variety of igneous, metamorphic and sedimentary soil
281 parent materials of varying age from across the northeastern US. For soils developed from
282 crystalline silicate rocks and some clastic non-carbonate sedimentary rocks, the 1 N HNO_3
283 extracts at 20°C consistently exhibited a Ca:P ratio similar to apatite. The presence of apatite for
284 these C horizon samples was confirmed for each soil by mineralogical analysis.

285 The sequential extraction studies of Nezat et al. (2007; 2008) suggest that the mineral
286 weathering end-member for the granitic soils at the La Ronge study site will be reliably
287 determined using the sequential extraction method. We thus decided to perform a sequential
288 extraction on lower B (or BC) horizons in each study plot following a similar protocol. By
289 investigating the relationships between the chemical and isotopic signatures of the extracts, we
290 may also identify the specific minerals being dissolved. The best soil horizon proxy for Ca release
291 from mineral weathering is difficult to determine for different reasons. The parent C horizon is a
292 better proxy of historical soil mineral weathering (i.e. after deglaciation) because, by definition, it
293 is the unweathered part of the soil profile. If very old Ca is still being recycled by the trees, then
294 using the parent C containing fresh apatite and perhaps calcite seems reasonable. However, the
295 trees are likely capturing Ca from a soil residuum (rooting zone) that changed over time, one that
296 contains less apatite and very likely no calcite [as indicated in surface mineral soils in the
297 northeastern US due to depletion by chemical weathering (Blum et al. 2002; Nezat et al. 2004;
298 2007; 2008)]. The soil horizon that most reflects these conditions is the upper B horizon, where
299 biochemical weathering reactions take place. Using this horizon is therefore the best proxy for
300 new Ca being added to the soil-plant system via soil mineral weathering. Because 80–90% of the
301 Ca in the trees at the site appears to be recycled (Holmden and Bélanger 2010), it seems
302 reasonable to select a horizon that captures both the historical and current flux of Ca from soil

mineral weathering. Thus, we chose the lower B (or BC) horizon because we felt it represents an intermediate stage of weathering. By doing so, there is the possibility that the $^{87}Sr/^{86}Sr$ of soil mineral weathering will be lower than that of the upper mineral soil, assuming depletion of apatite in the upper B, as the Sr in apatite is less radiogenic than the Sr in biotite and chlorite. If depletion of apatite relative to phyllosilicates has indeed occurred, then this would mean that the soil mineral weathering inferred from the lower B horizons is a better proxy of 'historical' weathering than 'current' weathering. Relative to the $^{87}Sr/^{86}Sr$ of rainwater and snow, it will be seen later that using a soil mineral weathering $^{87}Sr/^{86}Sr$ signature that reflects past weathering is conservative with respect to calculating the contribution of the atmospheric flux to Sr and Ca pools in trees.

The sequential extracts used in this study are as follows: a 3 g sample was first leached for 2 hours on an end-over-end shaker with 30 ml of 0.1 M $BaCl_2$ solution to remove exchangeable Ca and Sr. The sample was then leached once more for 2 hours on the same shaker with 30 ml of 1 N HNO_3 at room temperature, maintained at 20-21˚C. The third step was to leach the 1 N HNO_3 leached soils in 50 mL centrifuge tubes with 15 N HNO_3 for ten hours in an oven at 80˚C. Finally, the residues of those sub-samples were transferred to individual PTFE beakers and completely consumed with a mixture of concentrated HF and HNO_3 acids for 48 hours on a hot plate at ~120˚C. The digests were evaporated to dryness and the residues re-dissolved in 0.2 N HNO_3 for analysis. A finely ground sample of the local granite was also subjected to the 1 M $BaCl_2$/1 N HNO_3/15 N HNO_3 sequential protocol described above, and another sample was dissolved completely in HF-HNO_3 for 48 hours.

Elemental and Isotopic Chemistry

Foliage and stemwood samples were oven-dried for 48 h at 65 ºC. The dried samples were then digested in ultra pure 15 N HNO_3 in a clean room environment and then evaporated

and resolubilized in 0.2 N HNO_3. Water samples, soil extracts/digests and plant digests were filtered through a 0.2 μm PTFE membrane. Base cations were determined by atomic absorption (Ca, Mg and Sr) and emission (K and Na) (Varian Spectr*AA* 220). Water samples were also analyzed for Cl^-, NO_3^-, SO_4^{2-} and PO_4^{3-} by ion chromatography (Waters), whereas PO_4^{3-} concentration on soil extracts and digests was determined colorimetrically (molybdenum blue) with a Technicon Auto-Analyzer. Samples for $^{87}Sr/^{86}Sr$ determination were passed through a quartz column packed with AG50 X-12 cation exchange resin to separate Sr from matrix cations. Purified aliquots of Sr (0.1 to 1 μg) were loaded onto single tantalum (Ta) filaments with a phosphoric acid and Ta gel mixture to increase ionization efficiency. Isotopic measurements of Sr were performed by thermal ionization mass spectrometry (Thermo Fisher Triton instrument) using a static multi-collection routine and a correction for instrumental mass fractionation using 0.1194 for $^{86}Sr/^{88}Sr$. The reproducibility of the analyses is better than ±25 ppm (2RSD) based on repeated measurements of samples, as well as quality control runs of NIST SRM 987, which yielded 0.710250 ±0.00014 throughout the course of this work. Samples containing low Sr and Ca concentrations (mostly precipitation and snow samples) were determined by isotope dilution thermal ionization mass spectrometry using a triple ^{84}Sr-^{42}Ca-^{48}Ca tracer (Holmden and Hudson 2003).

Mass Balance for Ca Apportionment Calculations

Equation 1 was used to calculate the fractions of atmospheric deposition and soil mineral weathering derived Ca in: (1) the trees from each plot using the weighted average $^{87}Sr/^{86}Sr$ ratios calculated from the Ca allometry and measured Sr/Ca ratios; and (2) the forest floor solutions whose $^{87}Sr/^{86}Sr$ ratios are dominantly controlled by Sr leached from relatively fresh litter. The only drawback to using the forest floor solution as a proxy for vegetation is that the Sr leached

from litter will be diluted somewhat by Sr in precipitation, which will cause $^{87}Sr/^{86}Sr$ ratios to be lower than in trees.

Equation 1:

$$\frac{Ca_a}{Ca_{veg}} = \frac{Ca_a}{Ca_a + Ca_w} = \frac{\left(\frac{Sr}{Ca}\right)_w \left[\left(\frac{^{87}Sr}{^{86}Sr}\right)_w - \left(\frac{^{87}Sr}{^{86}Sr}\right)_{veg}\right]}{\left(\frac{Sr}{Ca}\right)_a \left[\left(\frac{^{87}Sr}{^{86}Sr}\right)_{veg} - \left(\frac{^{87}Sr}{^{86}Sr}\right)_a\right] + \left(\frac{Sr}{Ca}\right)_w \left[\left(\frac{^{87}Sr}{^{86}Sr}\right)_w - \left(\frac{^{87}Sr}{^{86}Sr}\right)_{veg}\right]}$$

where *veg* is for the weighted average ratio in the trees from each plot, *a* is the mean weighted ratio of bulk precipitation, and *w* is for soil mineral weathering $^{87}Sr/^{86}Sr$ as deduced from the 1 N and 15 N HNO_3 extracts of the lower B horizons. Calculations were performed (and presented) using data from both extracts as a means of accounting for the uncertainties associated with assigning a single soil mineral weathering $^{87}Sr/^{86}Sr$ in polymineralic soils (see DISCUSSION section for full details). Ca_{veg} is replaced with Ca_{FF} in Equation 1 for the calculations that used the forest floor (FF) $^{87}Sr/^{86}Sr$ as the 'mixed ratio'.

RESULTS

All $^{87}Sr/^{86}Sr$ data along with selected Ca and Sr concentrations and Sr/Ca ratios for rainwater, snow, soil solutions, shallow groundwater, soil extracts/digests, streamwater and plant tissues (foliage and stemwood) are presented in Table 4. These data are also plotted in Figures 2 to 6.

Atmospheric Deposition

The chemistry and $^{87}Sr/^{86}Sr$ ratios of wet-only deposition, bulk deposition and snow are presented in Table 4. Mean Ca concentrations, Sr concentrations, $^{87}Sr/^{86}Sr$ and Sr/Ca ratios range

between 0.27 and 0.38 mg l^{-1}, 0.79 and 3.44 µg l^{-1}, 0.7143 and 0.7177, and 1.38 and 4.36 millimoles/mole, respectively. Mean Sr concentration in bulk deposition collected in the forest gaps is the highest, whereas snow samples have the lowest mean concentration. Conversely, snow samples show the highest mean $^{87}Sr/^{86}Sr$ and Sr/Ca ratios. The mean weighted $^{87}Sr/^{86}Sr$ and Sr/Ca ratios of bulk precipitation are respectively 0.7156 ±0.013 1σ (30% winter and 70% summer precipitation) and 3.24 millimoles/mole. The relatively high $^{87}Sr/^{86}Sr$ ratio of atmospheric deposition is typical of $^{87}Sr/^{86}Sr$ measurements of continental precipitation [e.g. Simonetti et al. (2000) for inland Quebec and Poszwa et al. (2004) for Sweden].

Bedrock and Soil Chemical and Mineralogical Properties

Bulk chemistry for the soils of the two toposequences is shown in Table 5. The bulk chemistry of the lower B (or BC) horizons in the high and mid-elevation plots on toposequence 1 is very close to the local granite, whereas the other plots show compositional effects associated with sediment reworking during the glaciolacustrine phase, or contributions from other sediment sources. The mineralogy estimated from the UPPSALA norms for both the granite and the high- and mid-elevation plots on toposequence 1 is: plagioclase (45–55%), quartz (26–34%), hornblende (5.5–9.0%), orthoclase (7.5–8.1%), muscovite (2.5–3.0%), epidote (1.9%), apatite (0.16–0.20%) and chlorite (0%; which, includes primary illite, trioctahedral vermiculite of primary type, and biotite). The UPPSALA estimated mineralogy for the soils at the bottom of the toposequences is: plagioclase (23–32%), quartz (32–36%), hornblende (8.0–12%), orthoclase (14–19%), muscovite (5.0–6.7%), epidote (1.1–1.8%), apatite (0.40–0.44%), and chlorite (2.6–6.0%). The mineralogy of the mid-elevation plot from toposequence 2 is between the modes of the bottom and upper plots of toposequence 1, whereas the high elevation plot of that toposequence falls within the range of values of the bottom plots for all minerals except apatite, which is 0.28%.

Microprobe analysis of plagioclase crystals in the granite yielded an albite fraction of 80%. Biotite and chlorite were observed in a thin section of the granite, and also confirmed by electron microprobe analysis. Biotite was not detected, however, by X-ray diffraction in the bulk soils, but was detected in the sand size fraction in the high- and mid-elevation plots of toposequence 1. The vermiculite/chlorite grouping was detected in the bottom plots and the high- and mid-elevation plots of toposequence 2, which is consistent with the UPPSALA mineralogy. Inconsistencies in hornblende concentrations were noted between the UPPSALA mineralogy and the X-ray diffraction/electron microprobe data, the analytical techniques failing to detect it in both the granite and soil samples. Yet, the UPPSALA norms yielded hornblende between 5.5 to 12%, depending on the plot. It is deduced that the hydration of hornblende by a hydrothermal fluid occurred after the granite was emplaced, and that this led to the conversion of primary hornblende into the secondary chlorite, epidote, and titanite clusters observed in backscattered X-ray images using the scanning electron microscope, and confirmed using electron microprobe. The UPPSALA norms failed to account for this alteration reaction because Ca is first allocated to hornblende and then to epidote. The calculated epidote percentage is therefore likely underestimated. The overestimation of hornblende also tends to decrease the normative phyllosilicate abundances because the allocation of magnesium to hornblende occurs before phyllosilicates.

Soil and Vegetation

Downslope trends in $^{87}Sr/^{86}Sr$ ratios of the soil solutions (Fig. 2) and trees (Fig. 3) are found in both toposequences, with lower $^{87}Sr/^{86}Sr$ ratios generally characterizing higher elevation plots. On toposequence 1, for example, the $^{87}Sr/^{86}Sr$ ratios in soil solutions of the high elevation plot are below 0.715 in both the forest floor and upper B horizons, between 0.719 and 0.722 in the mid-elevation plot, respectively, and above 0.729 in the bottom plots, including groundwater

at 1.4 and 1.8 m depths. The Sr/Ca ratios vary little in the soil solutions and no trend can be observed along the slope of both toposequences: forest floor solutions range between 2.2 and 4.0 millimoles/mole, mineral soil solutions range between 3.3 and 5.6 millimoles/mole and shallow groundwaters range between 2.8 and 3.6 millimoles/mole (Table 4).

A cross-plot of $^{87}Sr/^{86}Sr$ ratios between foliage and stemwood shows the expected high degree of correlation (Fig. 4a). Similar cross-plots of $^{87}Sr/^{86}Sr$ between (1) trees and the forest floor solutions (Fig. 4b) and (2) forest floor and upper B solutions (Fig. 4c) exhibit more scatter, thus indicating that sources other than recent litterfall contribute Sr (and Ca) to the forest floor and upper B horizons, such as atmospheric deposition and soil mineral weathering, respectively. The variation in Sr/Ca ratios in the wood and foliage components is relatively small across the plots and no downslope trends are observed along the slopes of both toposequences (Table 4). Mean Sr/Ca ratios range from 2.6 to 6.8 millimoles/mole for wood, and from 1.4 to 3.3 millimoles/mole for foliage. The highest Sr/Ca ratio of 6.8 millimoles/mole is from the high elevation plot of toposequence 2 where the single wood sample analyzed for Ca and Sr concentrations may not be fully representative of the trees in that plot. Sr/Ca ratios in wood are generally higher than Sr/Ca ratios in foliage (Table 4).

Mineral Soil (Lower B or BC) Extracts

Cations were released from lower B horizons using ion exchange ($BaCl_2$) and acid leaching (HNO_3 and HF) in order to deduce the $^{87}Sr/^{86}Sr$ signature of soil mineral weathering in each plot (Fig. 4). Beginning with the $BaCl_2$ extractions, and taking the broadest possible view of the data from all six plots, the range in $^{87}Sr/^{86}Sr$ ratios extracted from the lower B horizons (0.711–0.730) overlaps soil solutions from the upper B horizon (0.711–0.732). Considering that one set of data represents the ion exchange pool and the other the soil solutions, and that the two types of soil data are from different depths in the soil profile, the similarity between them most

likely reflects the downward migration of Sr from upper B to lower B horizons and its retention on ion exchange sites (Table 4). Downslope trends in $^{87}Sr/^{86}Sr$ ratios characterize the soil extracts of toposequence 1, with lower $^{87}Sr/^{86}Sr$ ratios in higher elevation plots (Fig. 5), similar to the hillslope trend in $^{87}Sr/^{86}Sr$ ratios found in trees.

Sr/Ca ratios show more variability and are much higher in the $BaCl_2$ extracts than in the acid leaches (Table 4). Sr/Ca ratios vary from 11 to 33 millimoles/mole in the high elevation plot of toposequence 1 and the two mid elevation plots, whereas the other three plots vary between 4 and 5 millimoles/mole. For comparison, the Sr/Ca ratios of upper B horizon soil solutions in all plots range between 3 and 6 millimoles/mole. The Sr/Ca ratios in the extracts are negatively correlated with effective cation exchange capacity. A small exchange pool might amplify the relatively small plant-induced fractionation between Ca and Sr during uptake by fine roots (see DISCUSSION for more details). Moreover, the soils of the three plots with high Sr/Ca ratios have similar mineralogy and coarse texture, leading to the possibility that the ion exchange properties of these soils are responsible for greater retention of Sr relative to Ca. However, the fact that the fine roots do not occupy the lower B horizons means that this situation has no impact on the Ca apportionment results.

The 1 N HNO_3 extract gives consistent results, yielding higher $^{87}Sr/^{86}Sr$ ratios than the forest floor, upper B, and vegetation components in all plots with the exception of the high elevation plot on toposequence 1 where the ratios overlap each other (Fig. 5a). Downslope trends in $^{87}Sr/^{86}Sr$ ratios characterize the 1 N HNO_3 leaches in toposequence 1, with lower $^{87}Sr/^{86}Sr$ ratios in higher elevation plots, similar to the previously described hillsope $^{87}Sr/^{86}Sr$ trends in the $BaCl_2$ extracts (Figs. 5, 6a,b). Sr/Ca ratios in the 1 N HNO_3 leaches show low variability (1.2 to 3.3 millimoles/mole) compared to the $BaCl_2$ extracts, and no trend is observed along the hillslopes of both toposequences (Table 4).

A strong relationship between $^{87}Sr/^{86}Sr$ and Ca/PO_4 ratios suggests that soil mineral weathering involves two end-member suites of minerals (Fig. 6a). The low Ca and high PO_4 end-

474 member is likely apatite, which is present in all of the soils. It is also the only relatively abundant
475 mineral with high PO_4 levels in granites. Using the equation for the best-fit line and a Ca/PO_4
476 ratio of 1.66 for pure apatite, the corresponding $^{87}Sr/^{86}Sr$ ratio is 0.7058 (Figure 6a). This is
477 consistent with the initial $^{87}Sr/^{86}Sr$ ratio of 0.7068 for the bulk granite (after correcting for *in situ*
478 growth of ^{87}Sr since its formation 1.85 billion years ago based on a rubidium content of 43 ppm).
479 The other component with high $^{87}Sr/^{86}Sr$ and high Ca/PO_4 ratios is difficult to deduce from Fig. 6a
480 alone. However, the strong positive correlation between $^{87}Sr/^{86}Sr$ ratios and K concentrations
481 (Fig. 6b) leads to biotite (along with alteration products chlorite and vermiculite) as the most
482 likely candidates for the radiogenic end-member in the 1 N HNO_3 extracts. This is very consistent
483 with Nezat et al. (2007) who found that apatite was the main mineral dissolved in 1 N HNO_3 at
484 20°C, but that hornblende and biotite were also dissolved in small amounts. Of the common
485 silicate minerals found in granites, however, biotite is relatively low in Ca. Mass balance
486 calculations show that if all of the PO_4 released in the 1 N HNO_3 extract is assigned to apatite,
487 then only 20 to 50% of the Ca may be directly attributed to apatite dissolution in all six plots. The
488 remaining Ca must come from another mineral, epidote being the most likely candidate. Epidote
489 was not present in any of the soil separates in Nezat et al. (2007). However, it is present in all of
490 the soils at the La Ronge study site, is 2–4 times more abundant than apatite, and possibly
491 weathers more quickly than apatite (Pettijohn 1941). As explained earlier, epidote likely
492 originates in part from the hydration of primary igneous hornblende by a hydrothermal fluid after
493 the granite was emplaced.

494 The fact that the 1 N HNO_3 extract of the lower B horizon in the high elevation plot of
495 toposequence 1 gave an unusually low $^{87}Sr/^{86}Sr$ ratio (0.7155) compared to the other plots led to
496 further investigations of this soil. XRF analysis and UPPSULA norms suggest that it mostly
497 resembles the granite and the mid elevation soil of the same toposequence in terms of its bulk
498 chemistry and mineralogy. It is also contains significantly more sand (50%) than either the mid
499 elevation or low elevation plots from the same toposequence. The $^{87}Sr/^{86}Sr$ ratio of apatite

500 (0.7068) will be similar to the initial $^{87}Sr/^{86}Sr$ ratio of the granite at the time of emplacement
501 because apatite is essentially Rb-free, and there is consequently no change in $^{87}Sr/^{86}Sr$ ratio
502 expected from ^{87}Rb decay. The higher 0.7155 ratio of the 1 N HNO_3 leach means that in addition
503 to Sr from apatite (0.7068), there was a small contribution from biotite and chlorite/vermiculite
504 intergrades, albeit much smaller than in the leaches of the middle and low elevation soils. We
505 reasoned that the coarser grain size fractions (sands) probably do not differ much in bulk
506 chemistry and mineralogy relative to the finer particles (silt and clay), but that differences in
507 specific surface area and reactivity to acids may be large (Stillings and Brantley 1995). To test
508 this hypothesis, we sieved the lower B horizon from the high elevation plot into two grain sizes
509 (fine sand, and silt and clay) and leached them again with 1 N HNO_3, this time for 20 hours as
510 originally proposed by Nezat et al. (2007), to see whether phyllosilicates would be attacked and
511 thus yield a higher $^{87}Sr/^{86}Sr$ ratio in the leachate. Indeed, the $^{87}Sr/^{86}Sr$ ratio for the 20–hour leach
512 of the fine sand fraction gave 0.732, and the silt and clay fraction yielded 0.725. The higher
513 $^{87}Sr/^{86}Sr$ ratio of the fine sand fraction may mean that more primary biotite and chlorite are
514 present in this fraction than in the silt and clay. We conclude that apatite dissolution in a 1 N
515 HNO_3 solution is probably faster than phyllosilicate dissolution for soils with high sand content,
516 which impacts the $^{87}Sr/^{86}Sr$ ratio of Sr released in the fast leaching experiments. A longer leach
517 with 1 N HNO_3 (Nezat et al. 2007) therefore appears to be better suited for this coarser soil.

518 The 15 N HNO_3 extracts produced higher $^{87}Sr/^{86}Sr$ ratios (0.739 to 0.823) than the 1 N
519 HNO_3 extracts, correlating positively with K/Na ratio. This suggests that vermiculite/chlorite
520 intergrades, which are only partially dissolved by the 1 N HNO_3 leach, are further dissolved in
521 this extract, along with minor orthoclase and microcline (Fig. 6c). Similarly, Nezat et al. (2007)
522 found that the 1 N HNO_3 extract at 200°C mostly dissolved biotite and chlorite with small
523 amounts of feldspars. Downslope trends in $^{87}Sr/^{86}Sr$ ratios characterize the 15 N HNO_3 leaches in
524 toposequence 1, with lower $^{87}Sr/^{86}Sr$ ratios in higher elevation plots, similar to the $BaCl_2$ and 1 N
525 HNO_3 extracts described above (Fig. 5, 6c,d). Like the 1 N HNO_3 extracts, the Sr/Ca ratios in the

526 15 N HNO_3 extracts show relatively low variability (1.8 to 3.8 millimoles/mole) compared to the
527 $BaCl_2$ extracts, and no trend is observed along the slopes of both toposequences (Table 4).
528 The $^{87}Sr/^{86}Sr$ ratios of the HF digests of the residual material are also positively
529 correlated with K/Na ratio, indicating potassium feldspar dissolution. However, the $^{87}Sr/^{86}Sr$
530 ratios (0.707–0.724) are much lower than the 15 N HNO_3 extract due to the dissolution of albite,
531 the main residuum in these soils (Fig. 6d). This is once more supported by the results of Nezat et
532 al. (2007) who found that the concentrated HF/HNO_3/HCl digest mostly dissolved plagioclase
533 and alkali feldspars. From mass balance considerations, albite must have a low $^{87}Sr/^{86}Sr$ ratio,
534 similar to apatite and, in turn, similar to the granite at the time of its formation (0.7068). The low
535 $^{87}Sr/^{86}Sr$ ratio of the soil residuum and whole-rock granite supports the fact that soils, tills, and the
536 reworked lacustrine sediments, are mostly derived from the local granite, as was originally
537 presumed on the basis of its large regional exposure.
538

539 ## Streamwater

540 The streamwater $^{87}Sr/^{86}Sr$ ratios on toposequence 1 varied between 0.7206 and 0.7217
541 (mean: 0.7213) and are significantly correlated to mean air temperature 1, 2 and 5 days prior to
542 the stream grab and to Mg/Ca ratios (Fig. 7a,b). We have no streamwater Sr isotopes data for
543 toposequence 2. The streamwater Ca/Sr varied between 3.16 and 3.68 millimoles/mole (mean:
544 3.44) on toposequence 1 and between 3.12 and 3.86 millimoles/mole (mean: 3.47) on
545 toposequence 2 (results not shown).
546

547 ## Apportionment Calculations

548 Apportionment results are listed in Table 6 for each plot and presented in relationship to
549 topographic elevation in Figure 8. The $^{87}Sr/^{86}Sr$ ratios of the end-members to mixing (along with

550 $^{87}Sr/^{86}Sr$ ratios in vegetation and the forest floor solutions in each study plot) are also plotted in
551 Fig. 5b.
552
553 ***Toposequence 1***
554 It seems reasonable to think that, in a coarse grained soil, the tree fine roots satisfy their
555 nutrient requirements *via* nutrients released in the soil solutions from the dissolution of the finer
556 and more reactive soil particles. Thus, if the $^{87}Sr/^{86}Sr$ ratio of the 1 N HNO_3 20 h leach of the silt
557 and clay fraction is used in the mixing equation, the forest Ca cycle of the high elevation plot is
558 overwhelmingly supplied by atmospheric deposition, making up at least 94% of the input Ca flux.
559 The 15 N HNO_3 extract yields similar results at 98%, whereas the 1 N HNO_3 20 h extract of the
560 fine sand fraction gives 96%. Calculations yield almost identical results for the forest floor
561 component. The range of $^{87}Sr/^{86}Sr$ ratios in the vegetation and forest floor end-members is
562 relatively small (0.714-0.718) and tends to be around the average ratio for atmospheric
563 deposition, meaning that the atmospheric contributions to individual trees is always dominant –
564 the trees with the more radiogenic signature still show over 90% of atmospherically derived Ca.
565 The $^{87}Sr/^{86}Sr$ ratio of the soil mineral weathering signature of the bulk upper B mineral
566 soil in the mid elevation plot (0.733 for the 1 N HNO_3 2 h extract) is clearly higher than in the
567 high elevation plot, despite similar bulk chemistry and mineralogy. This is possibly due to the
568 greater content of fine particles in this soil, which favors more phyllosilicate dissolution at lower
569 acid strengths. Using 0.733 as the weathering end-member in the mixing equation yields an
570 atmospheric Ca contribution of 70% for the weighted average $^{87}Sr/^{86}Sr$ ratio in trees and 53% for
571 the Ca pool of the forest floor. The contributions are about 20% greater when the $^{87}Sr/^{86}Sr$ ratio of
572 the 15 N HNO_3 leach is used as the mineral weathering end-member.
573 The weighted average $^{87}Sr/^{86}Sr$ ratio in trees is 0.725 in the lowest plot (1.3). This ratio is
574 lower than the $^{87}Sr/^{86}Sr$ of the forest floor solution of 0.730. The $^{87}Sr/^{86}Sr$ ratio of the water in the

lysimeter is at the upper end of the range of $^{87}Sr/^{86}Sr$ ratios in the trees, similar to the mid elevation plot. It is important to note that the cohort of trees in this plot is dominated by a single large white spruce with a $^{87}Sr/^{86}Sr$ ratio of 0.722. We propose that the massive canopy from this single tree behaves as an effective filter of dry atmospheric deposition, and that the forest floor surrounding this tree benefits from higher atmospheric inputs with low $^{87}Sr/^{86}Sr$ ratios in throughfall and stemflow. This mechanism possibly explains the wide range of $^{87}Sr/^{86}Sr$ ratios recorded in the trees of this plot. The lysimeter station failed to capture this effect because it fell outside the zone of influence of the white spruce.

The $^{87}Sr/^{86}Sr$ ratio of the 1 N HNO_3 extract of the lower B horizon of the low elevation plot yielded 0.747, likely due to the high phyllosilicate content of this finer textured soil. Using this value in the mixing equation, several values for the atmospheric deposition contribution to this plot may be determined. If the forest floor solution is more representative of Ca cycling in bottom plots without large trees, then the application of the mixing equation yields an atmospheric Ca contribution of 47%. Applying the mixing equation to the weighted average $^{87}Sr/^{86}Sr$ ratio of vegetation yields 63%, owing to the influence of the large white spruce. The contributions are respectively 32% and 23% greater when the $^{87}Sr/^{86}Sr$ ratio of the 15 N HNO_3 leach is used. If the mixing equation is applied to the white spruce alone, then 74% of the Ca in this tree is derived from atmospheric sources using the $^{87}Sr/^{86}Sr$ ratio of the 1 N HNO_3 extract as the mineral weathering end-member. A similarly high contribution of atmospherically derived Ca is calculated for a balsam poplar sampled slightly outside of this plot, which also towers above the black spruce/aspen canopy.

Toposequence 2

The range of $^{87}Sr/^{86}Sr$ ratios in vegetation (0.717–0.719) brackets the forest floor solution of 0.718 in the high elevation plot (2.1). Using the weathering end-member of 0.737 in the mixing

600 equation, as indicated by the 1 N HNO_3 leach of the lower B horizon, yields large atmospheric
601 contributions of 84% and 86% to the Ca pools in trees and forest floor solutions, respectively.
602 The contributions increase by 12-13% if the $^{87}Sr/^{86}Sr$ ratio of the 15 N HNO_3 leach is used
603 instead.

604 The range of $^{87}Sr/^{86}Sr$ ratios in trees from the mid elevation plot is 0.727–0.730 and all
605 ratios are higher than the forest floor solution of 0.722. It would seem that the measurements of
606 just two samples of foliage and one sample of stemwood were not enough to characterize the
607 range of $^{87}Sr/^{86}Sr$ ratios in the trees of this plot, or that the placement of the lysimeter failed to
608 capture the $^{87}Sr/^{86}Sr$ ratio of average litterfall. Using the $^{87}Sr/^{86}Sr$ ratio of the 1 N HNO_3 extract of
609 0.736 in the mixing equation, atmospherically derived Ca is 31% in the trees and 62% in the
610 forest floor solution. The atmospheric contribution increases respectively by 55% and 31% when
611 using the $^{87}Sr/^{86}Sr$ ratio of the 15 N HNO_3 extract of 0.823.

612 The average $^{87}Sr/^{86}Sr$ in the trees in the low elevation plot of toposequence 2 is 0.729,
613 which is identical to the forest floor solution. Moreover, the variability in $^{87}Sr/^{86}Sr$ ratios in the
614 trees is very small when compared to the low elevation plot in toposequence 1 (1.3), which has a
615 single large tree that towers over the black spruce and aspen canopy. The 1 N HNO_3 leach yielded
616 0.739. Adopting this value for the weathering flux in the low elevation plot and applying the
617 mixing equation to the vegetation and the forest floor solution yields atmospherically derived Ca
618 contributions of 37% and 36%, respectively. Applying the $^{87}Sr/^{86}Sr$ ratio of the 15 N HNO_3
619 extract respectively increases the atmospheric contribution to 74% and 73%.

620

621 # DISCUSSION

622 ## *Soil Mineral Weathering Isotopic Signature and Uncertainties*

623 It is concluded that the 1 N HNO_3 extract mostly dissolves apatite, epidote and
624 vermiculite/chlorite intergrades: PO_4 is controlled by apatite, Ca is controlled by apatite and

625 epidote, and K is controlled by phyllosilicates. Apatite and biotite are recognized as being
626 important sources of Ca (Wallander et al. 1997; van Breemen et al. 2000a; b; Blum et al. 2002)
627 and K (Wallander 2000; Richter and Markewitz 2001) to trees, respectively. Because epidote
628 weathers quickly, it is also a potentially significant source of Ca to trees. On the other hand, the
629 15 N HNO_3 extract appears to attack vermiculite/chlorite intergrades as well as more resistant
630 minerals such as microcline and orthoclase that release nutrients more slowly and have small
631 amounts of Ca in them. The fact that the streamwater $^{87}Sr/^{86}Sr$ ratio augments with increasing air
632 temperature suggests that the more radiogenic minerals such as phyllosilicates and K-feldspars
633 are more readily dissolved at the higher soil temperatures of July and August, when the trees are
634 actively absorbing nutrients and growing. The relatively strong positive relationship between
635 $^{87}Sr/^{86}Sr$ and Mg/Ca of streamwater samples collected from June to October further suggests that
636 the increase in stream $^{87}Sr/^{86}Sr$ ratios during July and August is particularly due to more intense
637 weathering of Mg-rich phyllosilicate minerals over Ca-containing minerals (e.g. apatite and
638 epidote, perhaps some plagioclase). In this respect, inferring the soil mineral weathering $^{87}Sr/^{86}Sr$
639 signatures using the data from the 1 N HNO_3 treatment seems reasonable for soil weathering
640 reactions occurring in summer (during the growing season). It is a treatment that has been
641 adopted by others working on recently glaciated soils in temperate forests (e.g., Blum et al. 2002).
642 However, a recent study of Ca isotope fractionation in plant and soil pools of the La
643 Ronge study site, performed on the same samples as the ones presented here for Sr isotopes,
644 highlights a problem of using weak acid digests (1 N HNO_3) on natural mineral soils (lower B or
645 BC horizons) to distinguish pristine weathering signatures (Holmden and Bélanger 2010). It was
646 found that many of the soil extracts and acid leaches of the lower soils exhibited the heavy Ca
647 isotope signature of plant uptake imparted to the Ca pools of the upper soil. The fact that this
648 heavy isotope signature is found in leaches of soils situated below the finely rooted horizons was
649 interpreted as evidence for a large downward flux of Ca (and by inference, Sr) from the upper to
650 lower soil pools. The Sr in this downward percolating (recycled) flux is dominantly sourced from

litterfall, which has a $^{87}Sr/^{86}Sr$ ratio that reflects mixing between soil mineral weathering and atmospheric deposition signatures. This recycled Sr is either adsorbed on ion exchange sites in soils, or incorporated into newly formed (alteration) minerals. In either case, it must be removed before the true $^{87}Sr/^{86}Sr$ signature of soil mineral weathering is revealed. Unlike $^{87}Sr/^{86}Sr$, the Ca isotope signatures are relatively uniform among the various soil minerals. It is therefore relatively easy to pick the point in the sequential leaching procedure when the bulk of the recycled Ca (and Sr) has been removed. Holmden and Bélanger (2010) reported that all of the $BaCl_2$ extracts and most of the 1 N HNO_3 leaches contained recycled Sr. Because recycled Sr contains Sr from atmospheric deposition (the least radiogenic contribution to the Sr pool in trees), the 1 N HNO_3 leach underestimates the true $^{87}Sr/^{86}Sr$ ratio of the soil mineral weathering end-member. In contrast, the more aggressive 15 N HNO_3 leaches display little or no evidence for recycled Ca or Sr.

It is apparent that the soil mineral weathering $^{87}Sr/^{86}Sr$ signature of each plot could be further constrained in experiments using ^{44}Ca and ^{40}Ca as guides. For example, different ion exchangers and acids could be employed, the number and duration of the acid leaching steps adjusted and even the temperature of the leaches experimented with in order to gently strip away the recycled Sr component from the soils, while leaving the pristine soil minerals intact. The Ca isotope study also lends support to the methods employed herein. Namely, that the $^{87}Sr/^{86}Sr$ signature of soil mineral weathering is bracketed between the 1 N and 15 N HNO_3 leaches in all study plots. The impact of this uncertainty in the soil mineral weathering end-members is readily evaluated in Table 6 where the Ca apportionment results for the trees and the forest floor solutions are calculated separately for the 1 N and 15 N HNO_3 treatments. Although the higher $^{87}Sr/^{86}Sr$ ratio for the weathering end-member (15 N HNO_3) increases the calculated fraction of atmospherically derived Ca in the vegetation and soil pools, it does not appreciably change the Ca apportionment pattern that relates to landscape position, which is discussed in the next section.

A second source of uncertainty relates to the tendency for trees to preferentially absorb Ca over Sr in acid soils and/or to carry more Ca to foliage relative to Sr via the transpiration stream, resulting in lower Sr/Ca ratios in foliage compared to wood (Bailey et al. 1996; Poszwa et al. 2000; Bullen and Bailey 2005; Dasch et al. 2007; Beauregard and Côté 2008). The problem is that the Ca apportioning calculations are performed using a mixing equation that assumes that the isotopes of Sr behave as a conservative proxy for Ca. If there are steps during the cycling of Sr and Ca between the soil and vegetation pools where the Sr/Ca ratio of recycled Sr and Ca is not a function of conservative mixing between soil mineral weathering and atmospheric deposition sources of Sr and Ca, then additional uncertainty is imparted to the Ca apportionment results. Although it is difficult to assign a specific uncertainty to this effect, an examination of the Sr/Ca ratios of the end-members to mixing can inform on whether it is likely to be significant. The seasonally averaged Sr/Ca ratio of atmospheric deposition is 3.2 millimoles/mole, whereas the soil mineral weathering flux from the 1 N HNO_3 leaches averaged over the six study plots is 2.2 millimoles/mole. Tight recycling of Sr and Ca between the vegetation and forest floor mixes Sr and Ca from atmospheric deposition and soil mineral weathering. The weighted average Sr/Ca ratio in the trees is 2.6 millimoles/mole, and forest floor solutions is 2.9 millimoles/mole. These values are fairly consistent with the conservative mixing hypothesis and, thus, the largest source of uncertainty is the assignment of the soil mineral weathering $^{87}Sr/^{86}Sr$ ratio.

Dominance of Atmospheric Deposition in the Ca pools of Boreal Shield Forests

Apportionment analysis of Ca using $^{87}Sr/^{86}Sr$ as a tracer shows that none of the trees in the study plots at the La Ronge site depend entirely on soil mineral weathering as a source of Ca. In this sense, they are like the temperate forests of central New Hampshire where 5–40% of the Ca in the vegetation is from atmospheric sources (Bailey et al. 1996; Blum et al. 2002; Bullen and

701 Bailey 2005), albeit shifted towards greater atmospheric contributions. If seasonally averaged Ca
702 concentrations in precipitation from La Ronge are used, then the annualized atmospheric Ca
703 deposition flux is about 1.0 kg ha^{-1}. The total atmospheric Ca deposition flux estimated by Shaw
704 and Vet (2006) for the La Ronge area is about two times higher at 1.9 kg ha^{-1} as it includes the
705 dry component. These fluxes are quite smaller than the annual nutritional needs of trees (5 to 10
706 kg ha^{-1}, depending of the plot) estimated from the allometric equations (Lambert et al. 2005) and
707 the data in Table 3. In this respect, the apportionment results need to be considered as the buildup
708 and recycling of atmospherically derived Ca in the soil-vegetation system rather than the direct
709 and large use of current atmospheric Ca inputs by the trees on an annualized basis. This is
710 supported by the Ca isotopes data in Holmden and Bélanger (2010) for the La Ronge study site
711 which suggest that 80 to 90% of the Ca in the trees is from a recycled litterfall source.

712 In the Hawaiian Islands, it has been known for some time that as soils age and become
713 more deeply weathered, trees and upper soil pools shift from mineral weathering dominance to
714 atmospheric dominance (e.g. Kennedy et al. 1998). On the Oregon Coast, where the soil parent
715 material is schist, and where the soils are not as evolved as the most weathered examples from
716 Hawaii, vegetation and soil pools are dominated by atmospherically derived Ca sources due to a
717 high deposition flux (Perakis et al. 2006). More recently, it was shown that Costa Rican forests
718 growing on deeply weathered mountain soils flecked with basaltic clasts are completely
719 dominated by soil mineral weathering sources of Ca (Bern et al. 2005). This is the case even
720 though sea spray is the main source of atmospherically derived Sr, the same as in Oregon, and
721 precipitation rate is ~5 m per year, which delivers a relatively large load of atmospherically
722 derived Sr (and Ca) to the forest. In Costa Rica, however, the soil mineral weathering dominance
723 is aided by the high tectonic uplift rate, which sustains high erosion rates (even for
724 geomorphologically old settings such as ridgetops and high plateaus), thus ensuring a continuous
725 supply of fresh fragments of easily weathered basalt for tree roots to use. These examples
726 demonstrate that it is relative rates of Ca and Sr inputs that decide whether atmospheric

727 deposition or soil mineral weathering sources will dominate the Ca and Sr cycles of the forests in
728 different regions.

729 The fact that the soils in the La Ronge study area are relatively easily weathered tills does
730 not appear to have any bearing on Ca sourcing by trees in this ecosystem, which is likely a
731 function of the harsh climate in northern Saskatchewan. Factors such as short growing seasons,
732 cool soil temperatures, low rainfall, and permafrost combine in boreal regions to create dry and
733 cool soils, thus limiting soil mineral weathering rates. As a general comparison, the mean annual
734 air temperature and rainfall in La Ronge are respectively –0.1ºC and 484 mm compared to 5.9ºC
735 and 1,400 mm for Lincoln, New Hampshire, which is close to the Hubbard Brook Experimental
736 site (Blum et al. 2002) and the Cone Pond watershed (Bailey et al. 1996; Bullen and Bailey
737 2005). Moreover, fine root density in the forest floor increases with increasing latitude between
738 Boreal Plain and Boreal Shield forests of Saskatchewan and Manitoba (Steele et al. 1997) (Fig.
739 1), suggesting fewer roots in the mineral soil for trees to satisfy their Ca requirements via soil
740 mineral weathering. Therefore, it seems likely that forests growing further north in the Taiga will
741 continue this trend, showing even higher proportions of atmospherically derived Ca in trees.

742 Despite the low rainfall, atmospheric Ca deposition rates in the Boreal Shield forests of
743 northern Saskatchewan are relatively high compared to eastern temperate and Boreal Shield
744 forests. The yearly total deposition flux of Ca in 1989 ranged from 1.2 to 1.4 kg ha^{-1} in the
745 southern half of the province of Quebec (Boulet and Jacques 1992) and it was on average 1.2 kg
746 ha^{-1} between 1987-1992 at the Hubbard Brook experimental site (Likens and Bormann 1995). As
747 mentioned above, the estimated total Ca deposition flux in the La Ronge area could be as high as
748 1.9 kg ha^{-1} y^{-1} (Shaw and Vet 2006). In a study on the impacts of a base metal smelter on the
749 southern edge of the Precambrian Shield at the Saskatchewan-Manitoba border, McMartin et al.
750 (1999) calculated that the winds were mostly coming from the North West but also noted a
751 frequency of about 30% of winds coming from the South, South West or South East. The
752 relatively high total Ca deposition rate at the site is therefore likely due to the influence of air

masses transporting calcareous dust from southern Saskatchewan, as indicated by estimates of yearly total Ca deposition rates as high as 2.7 kg ha^{-1} in the southern parts of the province (Shaw and Vet 2006). Therefore, the apportionment results at the La Ronge site could depend not only on the low flux magnitude of Ca from soil mineral weathering, but on the relatively high amount of Ca carried as dust from the southern plains.

Landscape Effects on the Apportioning of Ca in Trees

Forests in the high elevation plots exhibit greater dependence on atmospherically derived Ca than those in middle and low elevation plots (Fig. 8). This influence of landscape on the apportioning of Ca and Sr in trees is a very interesting and surprising finding of the study. It is particularly evident when using the $^{87}Sr/^{86}Sr$ ratio of the 1 N HNO_3 extract as the soil mineral weathering signature, whereas it is softened when using the $^{87}Sr/^{86}Sr$ ratio of the 15 N HNO_3 extract. In the latter case, atmospheric contributions to the Ca pools in trees are even more dominant (between 74% and 98%), but a decreasing trend of the atmospheric contribution is still seen from top to bottom. We offer two explanations to support this finding, both of which are likely concomitantly active.

First, if each plot is assumed to receive a constant supply of atmospherically derived Ca, then hillslope changes in soil mineral weathering rates are required to explain the changing proportions of atmospherically derived Ca cycling internally within each plot. Coarser soils are expected to release less Ca from mineral weathering than finely textured (heavy) soils because coarser soils generally present a smaller total surface area to weathering (Anbeek et al. 1994; Hodson 1998). Coarse soils also retain less water for chemical reactions to take place (Birkeland 1984) and moist soils are essential for carbonic acid formation and fine root vigor, activities that enhance soil mineral weathering (Ochs et al. 1993; Calvaruso et al. 2006). This could explain why the trees growing on the coarser soil of the high elevation plot on Toposequence 1 contain

778 more atmospherically derived Ca in their tissues than the trees growing on the heavier soil of the
779 low elevation plot. Changes in the proportions of the more easily weathered Ca-containing
780 minerals could also be a cause for differences in soil mineral weathering rates along the slope. In
781 this respect, it is reasonable to suggest that the impact of landscape on soil mineral weathering,
782 even on short slopes like the ones studied in the La Ronge area, is large enough to potentially
783 affect the apportionment of Ca by the trees. Similarly, Nakano et al. (2001) studied a forested
784 hillslope in Japan that covered 74 m of slope and 28 m of elevation. Using $^{87}Sr/^{86}Sr$ as a tracer, it
785 was determined that trees growing near the stream received ~40% of their Ca from atmospheric
786 sources, while those at higher elevation received 80%. The authors attributed this finding to
787 changes in the chemical and mineralogical characteristics of the volcanic ash soils along the
788 hillslope. However, in this study, it seems less likely that the Ca apportionment results are solely
789 due to hillslope changes in soil properties and mineral weathering. This is particularly true of
790 toposequence 2 where there are slope related changes in soil texture and mineralogy which are
791 less consistent with the apportionment results than for toposequence 1.
792 We therefore offer a second explanation: hilltop canopies are better suited to filtering
793 atmospheric aerosols because they are better exposed to atmospheric circulation than shielded
794 canopies in the valley floors. The captured aerosols are transferred to the forest floor as
795 throughfall and stemflow. According to the canopy filter hypothesis, the high elevation plot of
796 toposequence 1 is in the best position to capture atmospheric aerosols. One would expect that the
797 proportion of atmospherically derived Ca in trees would be high because they occupy the highest
798 position in the watershed in addition to being supported by sandy and dry soil to slowly release
799 Ca from mineral weathering. A case in point is the high atmospherically derived Ca contribution
800 of 84% calculated for the top of toposequence 2, which is characterized by a soil similar to those
801 of the low elevation plots but is only 2 m lower in elevation than the high elevation plot on
802 toposequence 1. It is therefore argued that canopy filtering may overwhelm soil mineral
803 weathering in the apportionment of Ca to trees, even in soils with high exchangeable reserves.

The notion that canopy height plays a role in capturing dry deposition can also be demonstrated in the bottom plots of both toposequences where soil mineralogy, texture, and $^{87}Sr/^{86}Sr$ signatures of soil mineral weathering are similar (0.739–0.747), but the size distribution among the cohort of trees is not. The plot with higher trees (i.e. the bottom plot of toposequence 1) records higher atmospherically derived Ca contributions in the vegetation and the forest floor. It would appear that tall trees with large canopies filter more dry particulates than surrounding shorter trees, which, in turn, affects Ca balances of atmospheric deposition and soil mineral weathering at the microsite level.

CONCLUSION

This work supports previous Sr and Ca cycling studies in other forest ecosystems suggesting that much of the Ca requirement in trees can be met *via* atmospheric deposition. Topography was found to be an important factor determining the extent to which trees sequester atmospherically derived Ca, with stands at higher elevation receiving a greater proportion of their Ca requirements through atmospheric deposition. The question arising from this finding is whether the landscape effect is due to changes in soil mineral weathering rates between hilltops and valley floors, or changes in atmospheric deposition rates by canopy filtering. More work is required to answer this question, with a focus on estimating rates of Sr and Ca supply to and from the system.

We do acknowledge that the conditions found at the study site may be specific to this region and suggesting a similar dominance of atmospheric Ca deposition for another area of the Boreal Shield in Canada may be a stretch. But the finding that the forests in the La Ronge study area use so much atmospheric Ca to satisfy their Ca requirement is perhaps understandable from the point of view that soils at the study site are cold and thaw only by the end of May, which means a shorter window for Ca to be released in the soil *via* mineral weathering. Moreover, the

fact that atmospheric Ca deposition rates are high due to the southern plains (or Prairie) influence, with large areas characterized by calcareous soils, needs to be considered. The warmer climate in boreal stands of eastern Canada, for example, could be a factor motivating larger soil mineral weathering contributions to their standing biomass because of greater soil mineral weathering and a smaller Ca flux from atmospheric deposition. We also predict that boreal forests located further north will lean even more towards atmospherically derived Ca sources owing to increasingly shorter growing seasons and permafrost dominance, which encourages fine root colonization of the forest floor over the mineral soil.

ACKNOWLEDGEMENTS

We thank J. Moukoumi and E. Thiffault for reviewing early drafts of this manuscript. We also thank A. Taylor, S. Friessen, M. Emigh, J. Jackson and N. Roberston for their hard work in the field and laboratory. This study was made possible by financial support to N. Bélanger from the Natural Science and Engineering Council of Canada (Discovery grant).

Acton, D. F., Padbury, G. A. and Shields, J. A. 1983. Soils of the Amisk-Cormorant lake area. Agriculture Canada, Land Resource Research Centre Contribution 87-45, Ottawa, Ontario.

Alban, D. H., Perala, D. A. and Schlaegel, B. E., 1978. Biomass and nutrient distribution in aspen, pine, and spruce stands on the same soil type in Minnesota. Can. J. For. Res. **8**: 290–299.

Anbeek, C., Van Breemen, N., Meijer, E. L. and Van Der Plas, L. 1994. The dissolution of naturally weathered feldspar and quartz. Geochim. Cosmochim. Acta. **58**: 4601–4613.

Ansdell, K. M., Heaman, L. M., Machado, N., Stern, R. A., Corrigan, D., Bickford, M. E., Annesley, I., Böhm, C. O., Zwanzig, H. V., Bailes, A. H., Syme, R., Corkery, T., Ashton, K. E., Maxeiner, R. O., Yeo, G. and Delaney G. D. 2005. Correlation chart of

854 the evolution of the Trans-Hudson Orogen Manitoba-Saskatchewan segment. Can. J. Earth
855 Sc. **42**: 761.
856 **Arocena, J. M. 2000.** Cations in solution from forest soils subjected to forest floor removal and
857 compaction treatments. For. Ecol. Manage. **133**: 71–80.
858 **Bailey, S. W., Hornbeck, J. W., Driscoll, C. T. and Gaudette, H. E. 1996.** Calcium inputs and
859 transport in a base-poor forest ecosystem as interpreted by Sr isotopes. Water Res.
860 Research **32**: 707–719.
861 **Beauregard, F. and Côté, B. 2008.** Test of soil extractants for their suitability in predicting
862 Ca/Sr ratios in leaves and stems of sugar maple seedlings. Biogeochemistry **88**: 195–203.
863 **Bern, C. R., Townsend, A. R. and Farmer, G. L. 2006.** Unexpected dominance of parent-
864 material strontium in a tropical forest on highly weathered soils. Ecology **86**: 626–632.
865 **Birkeland, P. W. 1984.** Soils and geomorphology. Oxford University Press, New York, New
866 York.
867 **Blum, J. D., Klaue, A., Nezat, C. A., Driscoll, C. T., Johnson, C. E., Siccama, T. G., Eagar,**
868 **C., Fahey,T. J. and Likens, G. E. 2002.** Mycorrhizal weathering of apatite as an
869 important calcium source in base-poor forest ecosystems. Nature **417**: 729–731.
870 **Boulet, G. and Jacques, G. 1992.** Programme d'échantillonnage des précipitations du Québec:
871 sommaire des données de la qualité des eaux de précipitations, 1989. Ministère de
872 l'Environnement du Québec, Rapport QEN/PA-45 de la Direction des réseaux
873 atmosphériques, Québec.
874 **Bullen, T. D. and Bailey, S. W. 2005.** Identifying calcium sources at an acid deposition-
875 impacted spruce forest: a strontium isotope, alkaline earth element multi-tracer approach.
876 Biogeochemistry **74**: 63–99.
877 **Calvaruso, C., Turpault, M.-P. and Frey-Klett, P. 2006.** Root-associated bacteria contribute to
878 mineral weathering and to mineral nutrition in trees: a budgeting analysis. Appl. Environ.
879 Microbiol. **72**: 1258-1266.

880 **Capo, R. C., Stewart, B. W. and Chadwick, O. A. 1998.** Strontium isotopes as tracers of
881 ecosystem processes: theory and methods. Geoderma **82**: 197–225.
882 **Dasch, A.A., Blum, J.D., Eagar, C., Fahey, T.J., Driscoll, C.T. and Siccama, T.G. 2008.** The
883 relative uptake of Ca and Sr into tree foliage using a whole-watershed calcium addition.
884 Biogeochemistry **80**: 21–41.
885 **Drouet, Th., Herbauts, J., Gruber, W. and Demaiffe, D. 2005.** Strontium isotope composition
886 as a tracer of calcium sources in two forest ecosystems in Belgium. Geoderma **126**: 203–
887 **2**23.
888 **Finer, L., Messier, C. and DeGrandpré, L.** 1997. Fine-root dynamics in mixed boreal conifer-
889 broad-leafed forest stands at different successional stages after fire. Can. J. For. Res. **27**:
890 304–314.
891 **Flanagan, P.W. and Van Cleve, K. 1983.** Nutrient cycling in relation to decomposition and
892 organic matter quality. Can. J. For. Res. **13**: 795–817.
893 **Forsythe, L.H. and Coates, H. 1971.** Nemeiben lake (East Half). Department of Mineral
894 Resources, Geological Sciences Branch, Precambrian Geology Division Map 115E,
895 Regina, Saskatchewan.
896 **Hendershot, W. H., Lalande, H. and Duquette, M. 2007.** Ion exchange and exchangeable
897 cations. Pages 197–206 *in* M. R. Carter and E. G. Gregorich, eds. Soil Sampling and
898 Methods of Analysis, 2nd edition. CRC Press, Boca Raton, Florida.
899 **Hodson, M. E. 1998.** Micropore surface area variation with grain size in unweathered alkali
900 feldspars: implications for surface roughness and dissolution studies. Geochim.
901 Cosmochim. Acta **21-22**: 3429–3435.
902 **Holmden, C. and Hudson, J. D. 2003.** $^{87}Sr/^{86}Sr$ and Sr/Ca investigation of Jurassic molluscs
903 from Scotland: Implications for paleosalinities and the Sr/Ca ratio of seawater. Geol. Soc.
904 Am. Bull. **115**: 1249–1264.
905 **Holmden, C. and Bélanger, N. 2010.** Ca isotope cycling in a forested ecosystem. Geochim.

Cosmochim. Acta **74**: 995–1015.

Kennedy, M. J., Chadwick, O. A., Vitousek, P. M., Derry, L. A. and Hendricks, D. M. 1998. Changing sources of base cations during ecosystem development, Hawaiian Islands. Geology **26**: 1015–1018.

Kennedy, M. J., Hedin, L. O. and Derry, L. A. 2002. Decoupling of unpolluted temperate forest from rock nutrient sources revealed by natural $^{87}Sr/^{86}Sr$ and ^{84}Sr tracer addition. Proc. North Am. Acad. Sc. **99**: 9639–9644.

Kimmins, J. P., Binkley, D., Chatarpaul, L. and de Catanzaro, J. 1985. Biogeochemistry of temperate forest ecosystems: Literature on inventories and dynamics of biomass and nutrients. Canadian Forest Service, Petawawa National Forest Institute Inf. Report PI-X-47E/F, Ottawa, Ontario.

Kirkwood, D. E. and Nesbitt, H. W. 1991. Formation and evolution of soils from an acidified watershed: Plastic Lake, Ontario, Canada. Geochim. Cosmochim. Acta **55**: 1295–1308.

Lambert, M.-C., Ung, C.-H. and Raulier, F. 2005. Canadian national tree aboveground biomass equations. Can. J. For. Res. **35**: 1996–2018.

Likens, G.E. and Bormann, F.H. 1995. Biogeochemistry of a forested ecosystem, 2nd edition. Springer-Verlag, New York.

Likens, G. E., Driscoll, C. T. and Buso, D. C. 1996. Long-term effects of acid rain: response and recovery of a forest ecosystem. Science **272**: 244–246.

MacDonald, J. D., Bélanger, N., Sauvé, S., Courchesne, F. and Hendershot, W. H. 2007. Collection and characterization of soil solutions. Pages 179-198 *in* M. R. Carter and E. G. Gregorich, eds. Soil Sampling and Methods of Analysis, 2nd edition. CRC Press, Boca Raton, Florida.

McMartin, I., Henderson, P. J. and Nielsen, E. 1999. Impact of a base metal smelter on the geochemistry of soils of the Flin Flon region, Manitoba and Saskatchewan. Can. J. Earth Sci. **36**: 141–160.

Miller, E. K., Blum, J. D. and Friedland, A. J. 1993. Determination of soil exchangeable-cation loss and weathering rates using Sr isotopes. Nature **362**: 438–441.

Nakano, T., Yokoo, Y. and Yamanaka, M. 2001. Strontium isotope constraint on the provenance of basic cations in soil water and stream water in the Kawakami volcanic watershed, central Japan. Hydrol. Proces. **15**: 1859–1875.

Nezat, C. A., Blum, J. D., Klaue, A., Johnson, C. E. and Siccama, T. G. 2004. Influence of landscape position and vegetation on long-term weathering rates at the Hubbard Brook Experimental Forest, New Hampshire, USA. Geochim. Cosmochim. Acta **68**: 3065–3078.

Nezat, C. A., Blum, J. D., Yanai, R. D., Hamburg, S. P. 2007. A sequential extraction to determine the distribution of apatite in granitoid soil mineral pools with application to weathering at the Hubbard Brook Experimental Forest, NH, USA. Appl. Geochem. **22**: 2406–2421.

Nezat, C. A., Blum, J. D., Yanai, R. D. and Park, B.B. 2008. Mineral sources of calcium and phosphorus in soils of the northeastern United States. Soil Sci. Soc. Am. J. **72**: 1786–1794.

Ochs, M., Brunner, I., Stumm, W. and Cosovic, B. 1993. Effects of root exudates and humic substances on weathering kinetics. Water Air Soil Pollut. **68**: 213–229.

Ojakangas, R. W. and Matsch, C. L. 1982. Minnesota's geology. University of Minnesota Press, Minneapolis, Minnesota.

Olsson, B. A., Bengtsson, J. and Lundkvist, H. 1996. Effects of different forest harvest intensities on the pools of exchangeable cations in coniferous forest soils. For. Ecol. Manage. **84**: 135–147.

Paré, D., Rochon, P. and Brais, S. 2002. Assessing the geochemical balance of managed boreal forests. Ecol. Indicators **1**: 293–311.

Perakis, S. S., Maguire, D. A., Bullen, T. D., Cromack, K., Waring, R. H. and Boyle, J. R. 2006. Coupled nitrogen and calcium cycles in forests of the Oregon Coast Range.

Ecosystems **9**: 63–74.

Pettijohn, F.J. 1941. Persistence of heavy minerals and geologic age. J. Geol. 49: 610–615.

Poszwa, A., Dambrine, E., Pollier, B. and Atteia, O. 2000. A comparison between Ca and Sr cycling in forest ecosystems. Plant Soil **225**: 299–310.

Poszwa, A., Ferry, B., Dambrine, E., Pollier, B., Wickman, T., Loubet, M. and Bishop, K. 2004. Variations of bioavailable Sr concentration and $^{87}Sr/^{86}Sr$ ratio in boreal forest ecosystems. *Role of biocycling, mineral weathering and depth of root uptake.* Biogeochemistry **67**: 1–20.

Richter, D. D. and Markewitz, D. 2001. Understanding soil change. Soil sustainability over millennia, centuries, and decades. Cambridge University Press, Cambridge, United Kingdom.

Shaw, M. and Vet, R. J. 2006. 1994–1998 average wet and dry deposition fields. Meteorological Service of Canada Report, Environment Canada, Toronto.

Simonetti, A., Gariépy, C. and Carignan, J. 2000. Pb and Sr isotopic compositions of snowpack from Québec, Canada: Inferences on the sources and deposition budgets of atmospheric heavy metals. Geochim. Cosmochim. Acta **64**: 5–20.

Soil Classification Working Group, 1998. The Canadian system of soil classification. Agriculture and Agri-Food Canada Publication 1646 (Revised), 3rd edition., NRC Research Press, Ottawa, Ontario.

Steele, S. J., Gower, S. T., Vogel, J. G. and Norman, J. M. 1997. Root mass, net primary production and turnover in aspen, jack pine and black spruce forests in Saskatchewan and Manitoba, Canada. Tree Physiol. **17**: 577–587.

Stillings L.L. and Brantley, S.L. 1995. Feldspar dissolution at 25ºC and pH 3: Reaction stoichiometry and the effect of cations. Geochim. Cosmochim. Acta. **59**: 1483–1496.

Strong, W. L. and La Roi, G. H. 1983. Rooting depths and successional development of selected boreal forest communities. Can. J. For. Res. **13**: 577–588.

Sverdrup, H. and Warfvinge, P. 1992. Critical loads. Pages 171-186 *in* P. Sandén and P. Warfvinge, eds. Modelling groundwater response to acidification. Swedish Meteorological and Hydrological Institute Report 5, Norrköping, Sweden.

Thiffault, E., Paré, D., Bélanger, N., Munson. A. D. and Marquis, F. 2006. Harvesting intensity in the boreal forest: impacts on soil nutrient availability and tree nutrition. Soil Sc. Soc. Am. J. **70**: 691–701.

Tryon, P.R. and Chapin, III, F.S. 1983. Temperature control over root growth and root biomass in taiga forest trees. Can. J. For. Res. **13**: 827–833.

van Breemen, N., Finlay, R., Lundström, U., Jongmans, A., Giesler, R. and Olsson, M. 2000a. Mycorrhizal weathering: A true case of mineral plant nutrition? Biogeochemistry **49**: 53–67.

van Breemen, N., Lundström, U. S. and Jongmans, A. G. 2000b. Do plants drive podzolization via rock-eating mycorrhizal fungi? Geoderma **94**: 163–171.

Vitousek, P. M., Kennedy, M. J., Derry, L. A. and Chadwick, O. A. 1999. Weathering versus atmospheric sources of strontium in ecosystems on young volcanic soils. Oecologia **121**: 255–259.

Wallander, H., Wickman, T. and Jacks, G. 1997. Apatite as a source of mycorrhizal and nonmycorrhizal *Pinus sylvestris*. Plant Soil **196**: 123–131

Wallander, H. 2000. Use of strontium isotopes and foliar K content to estimate weathering of biotite induced by pine seedlings colonised by ectomycorrhizal fungi from two different soils. Plant Soil **222**: 215–229.

Watmough, S. A., Aherne, J., Alewell, C., Arp, P., Bailey, S., Clair, T., Dillon, P., Duchesne, L., Eimers, C., Fernandez, I., Foster, N., Larssen, T., Miller, E., Mitchell, M. and Page, S. 2005. Sulphate, nitrogen and base cation budgets at 21 forested catchments in Canada, the United States and Europe. Environ. Monitor. Assess. **109**: 1–36.

Weetman, G. F. and Webber, B. 1972. The influence of wood harvesting on the nutrient status of two spruce stands. Can. J. For. Res. **2**: 351–369.

LIST OF FIGURES

LIST OF TABLES

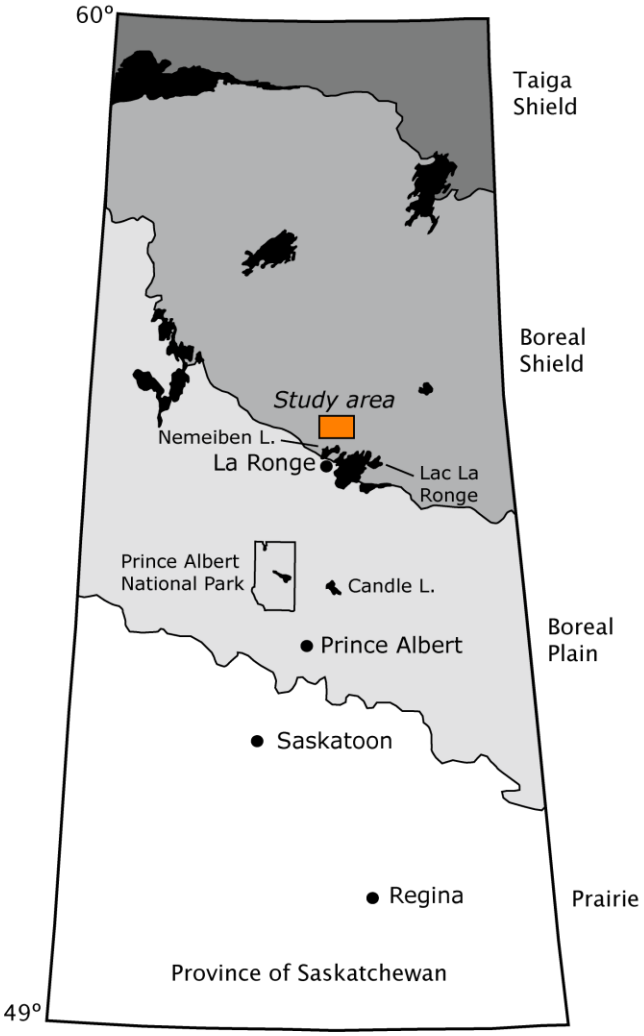
60°
Taiga
Shield
Boreal
Shield
Study area
Nemeiben L.
La Ronge
Lac La
Ronge
Prince Albert
National Park
Candle L.
Prince Albert
Boreal
Plain
Saskatoon
Regina
Prairie
Province of Saskatchewan
49°

Figure 1.

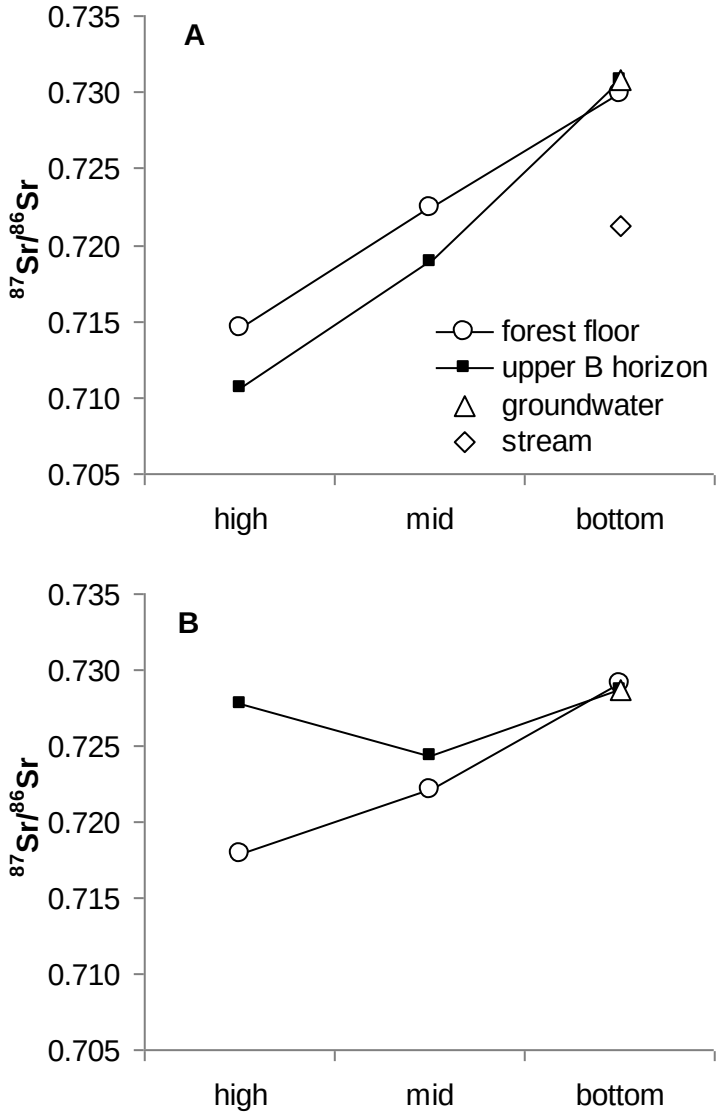
A
0.735
0.730
0.725
0.720
0.715
0.710
0.705
87Sr/86Sr
high
mid
bottom
forest floor
upper B horizon
groundwater
stream
B
0.735
0.730
0.725
0.720
0.715
0.710
0.705
87Sr/86Sr
high
mid
bottom

Figure 2.

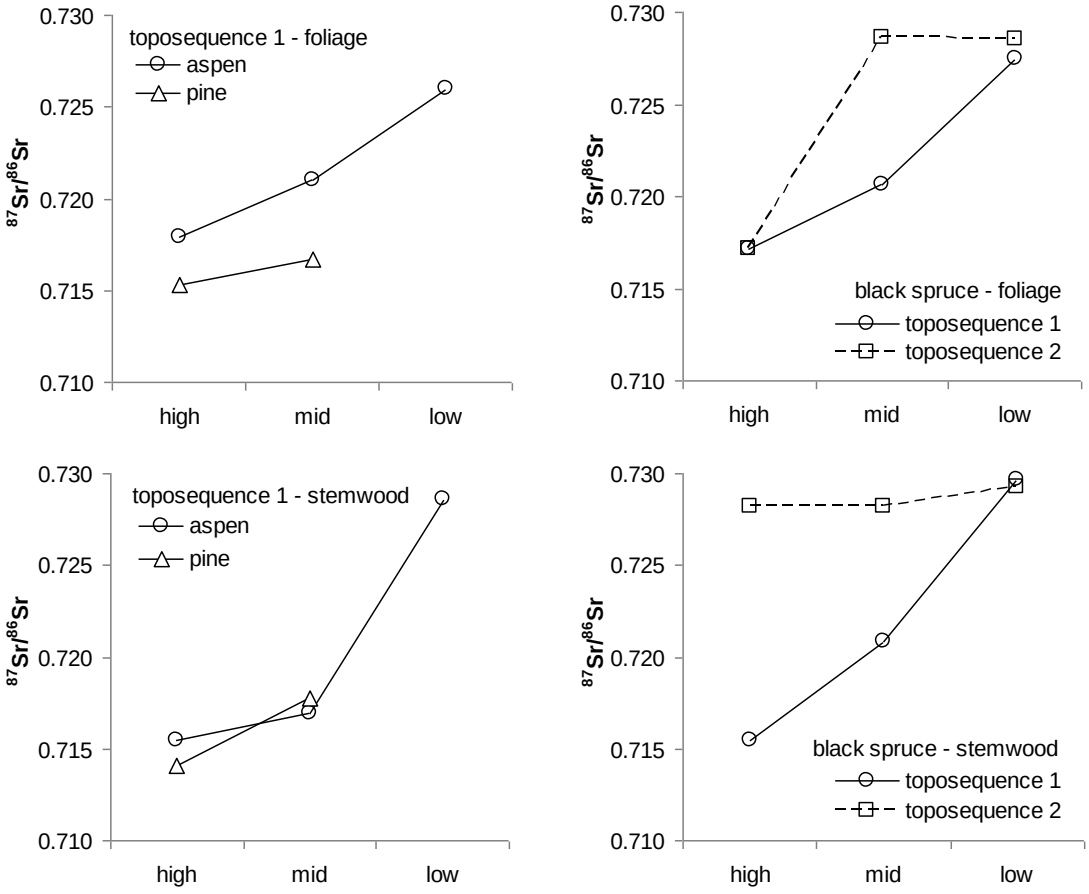
toposequence 1 - foliage
aspen
pine
black spruce - foliage
toposequence 1
toposequence 2
toposequence 1 - stemwood
aspen
pine
black spruce - stemwood
toposequence 1
toposequence 2
$^{87}Sr/^{86}Sr$
0.730
0.725
0.720
0.715
0.710
high
mid
low

Figure 3.

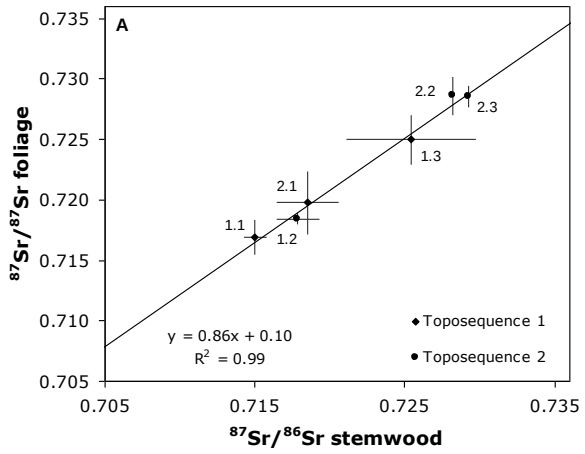
A
0.735
0.730
0.725
0.720
0.715
0.710
0.705
0.705
0.715
0.725
0.735
$^{87}Sr/^{87}Sr$ foliage
$^{87}Sr/^{86}Sr$ stemwood
2.2
2.3
1.3
2.1
1.1
1.2
y = 0.86x + 0.10
R^2 = 0.99
Toposequence 1
Toposequence 2

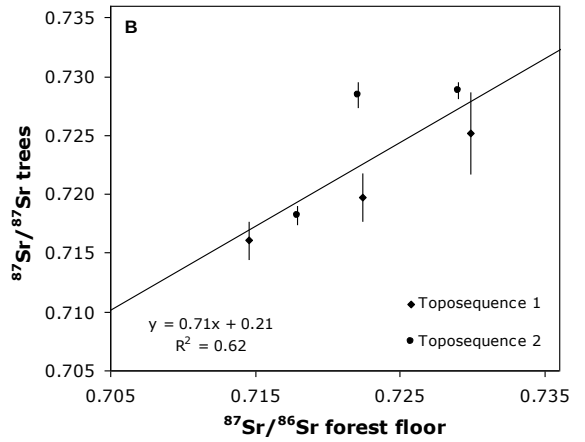
B
0.735
0.730
0.725
0.720
0.715
0.710
0.705
0.705
0.715
0.725
0.735
$^{87}Sr/^{87}Sr$ trees
$^{87}Sr/^{86}Sr$ forest floor
y = 0.71x + 0.21
R^2 = 0.62
Toposequence 1
Toposequence 2

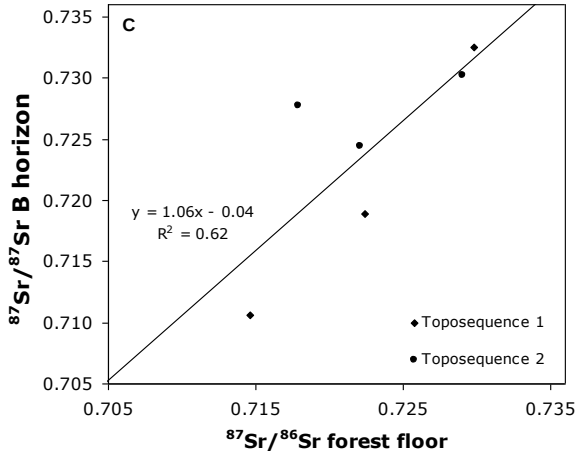
C
0.735
0.730
0.725
0.720
0.715
0.710
0.705
0.705
0.715
0.725
0.735
$^{87}Sr/^{87}Sr$ B horizon
$^{87}Sr/^{86}Sr$ forest floor
y = 1.06x - 0.04
R^2 = 0.62
Toposequence 1
Toposequence 2

Figure 4.

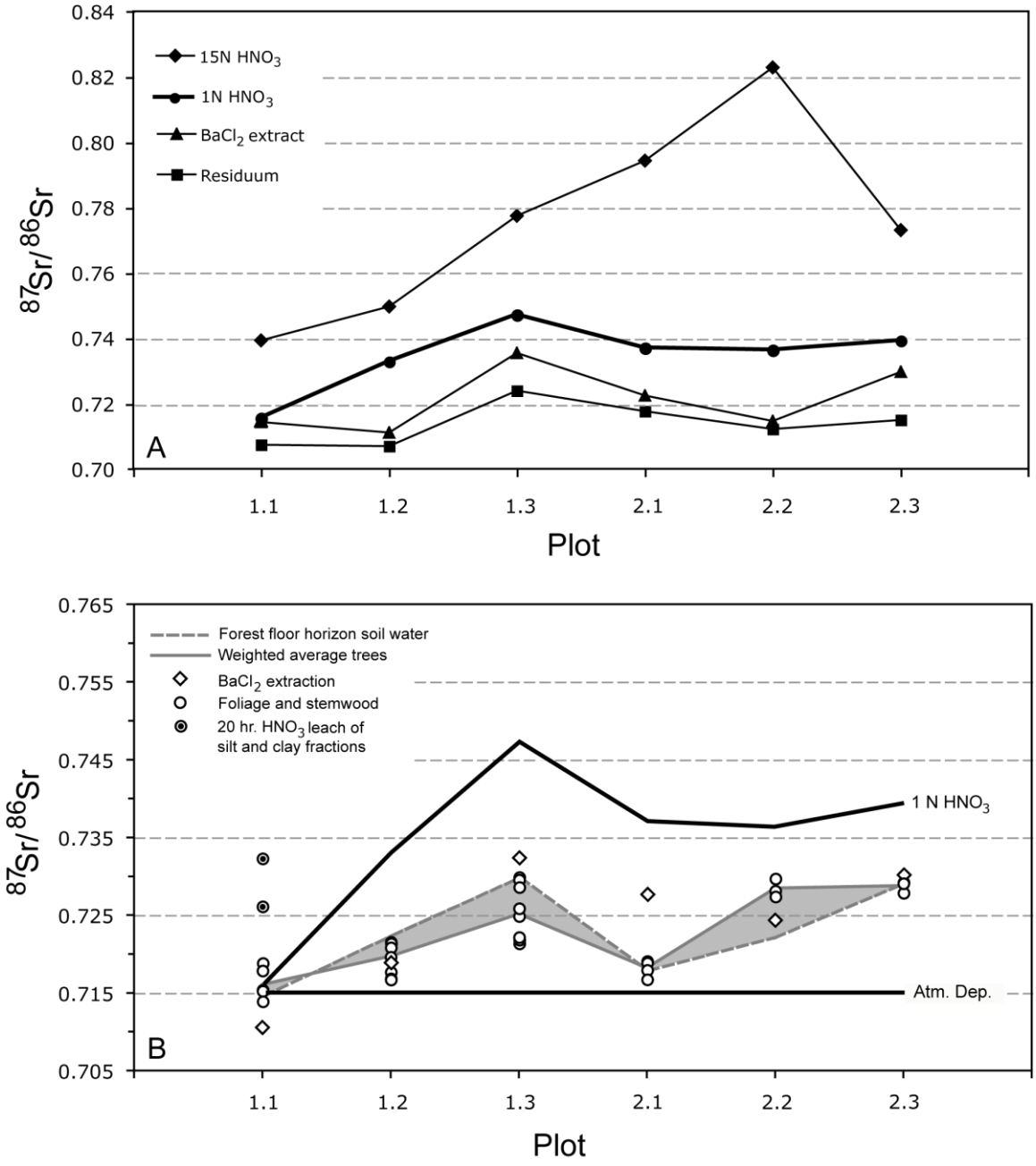
15N HNO3
1N HNO3
BaCl2 extract
Residuum
87Sr/86Sr
0.84
0.82
0.80
0.78
0.76
0.74
0.72
0.70
A
1.1
1.2
1.3
2.1
2.2
2.3
Plot
Forest floor horizon soil water
Weighted average trees
BaCl2 extraction
Foliage and stemwood
20 hr. HNO3 leach of silt and clay fractions
1 N HNO3
Atm. Dep.
0.765
0.755
0.745
0.735
0.725
0.715
0.705
B

Figure 5.

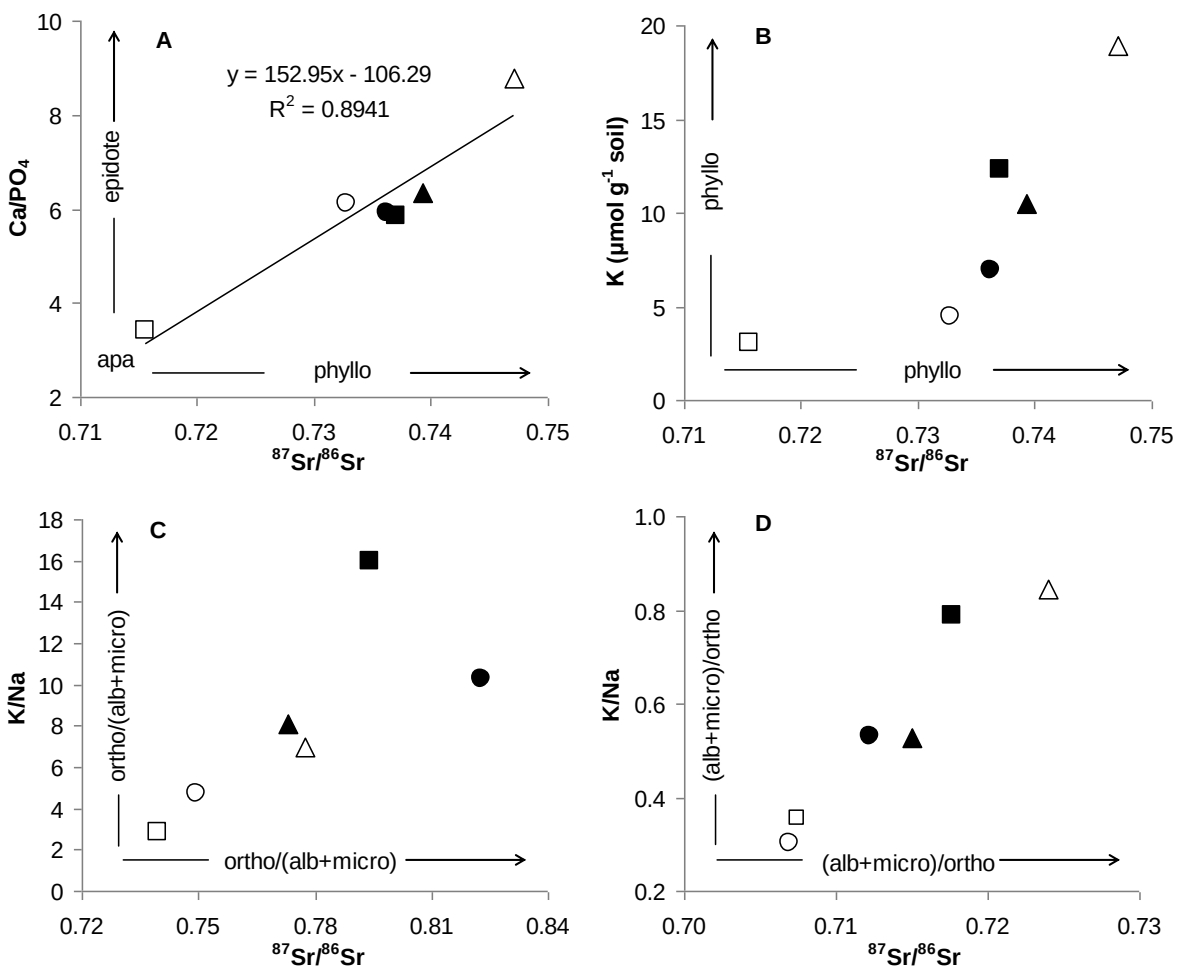
A
y = 152.95x - 106.29
R2 = 0.8941
Ca/PO4
epidote
apa
phyllo
87Sr/86Sr
B
K (µmol g-1 soil)
phyllo
phyllo
87Sr/86Sr
C
K/Na
ortho/(alb+micro)
ortho/(alb+micro)
87Sr/86Sr
D
K/Na
(alb+micro)/ortho
(alb+micro)/ortho
87Sr/86Sr

Figure 6.

1274

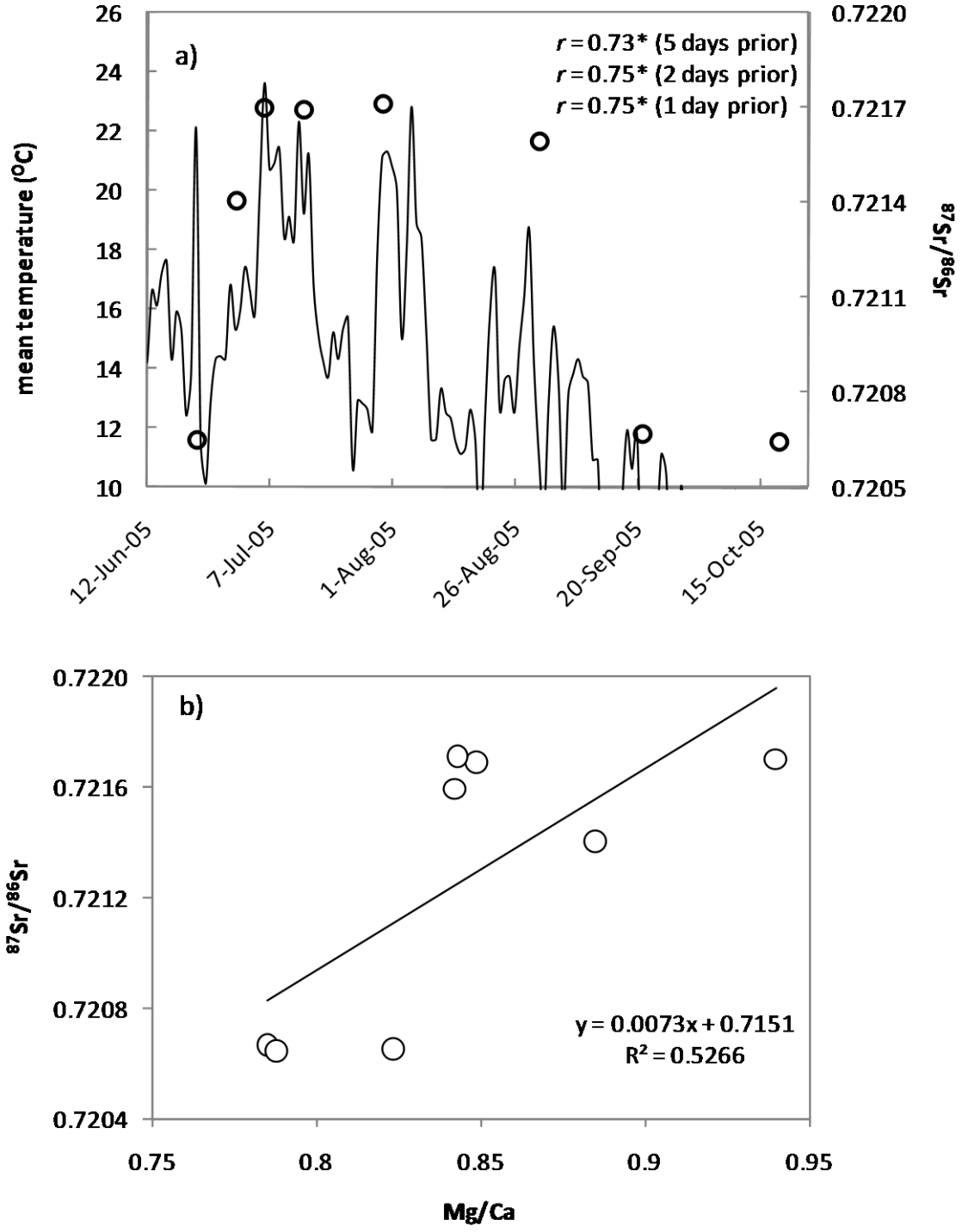

1275
1276
1277
1278 Figure 7.
1279
1280
1281

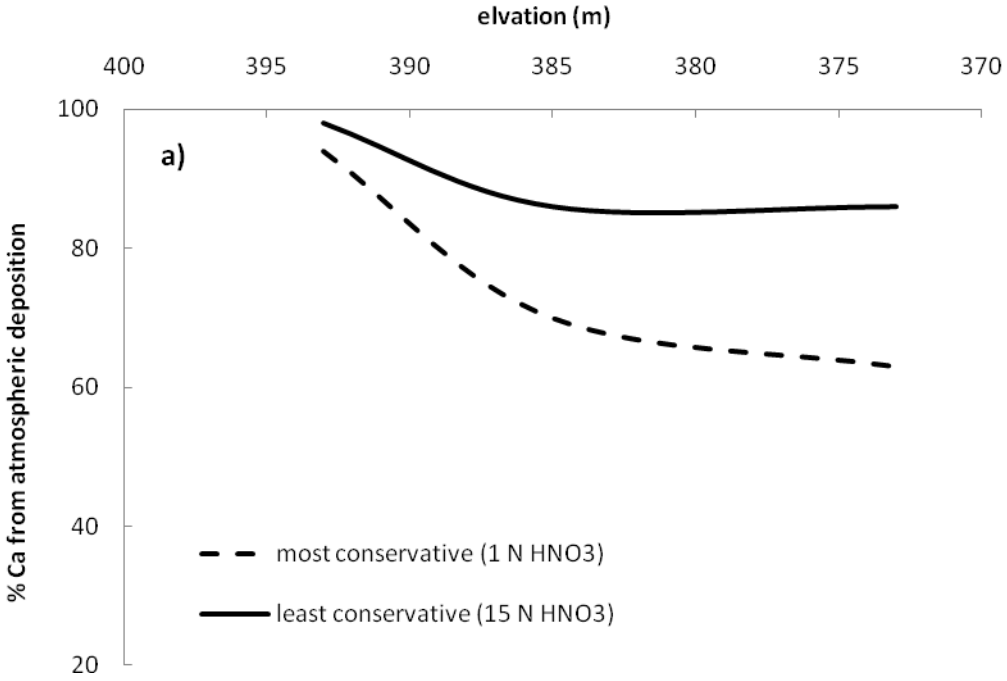

1282

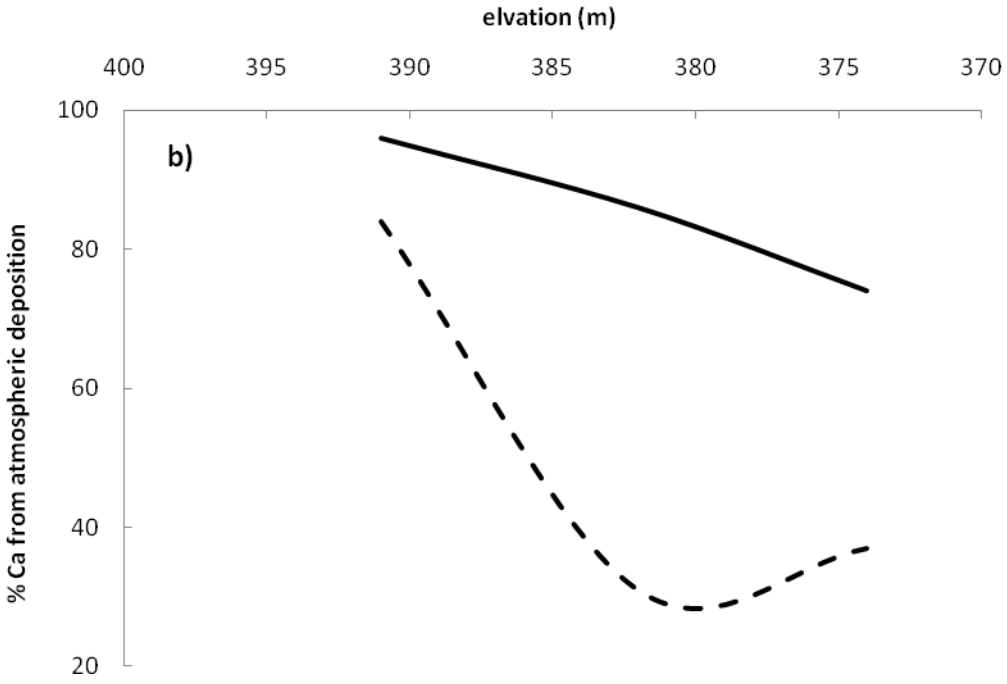

1283
1284
1285
1286 Figure 8.
1287

Table 1.

Source	Location	Tree species	Soil forming bedrock	Mineral weathering $^{87}Sr/^{86}Sr$	Atmospheric deposition $^{87}Sr/^{86}Sr$	Atmospherically-derived Ca pools (%)
Perakis et al. (2006)	Oregon Coast, USA	*Pseudotsuga menziesii*	sandstone	0.7217	0.7092	>97%
Kennedy et al. (2002)	Chilean Andes	*Nothofagus nitida*	mica-schist	0.7134	0.7092	>80%; mean: 91%
		Drimys winteri	mica-schist	0.7134	0.7092	>87%[1]
Kennedy et al. (1998)	Hawaii	*Metrosideros polymorpha*	0.3-2 ka basalt	0.7034	0.7093	5-10%
		Metrosideros polymorpha	20-4100 ka basalt	0.7034	0.7093	75-90%
Drouet et al. (2005)	Belgium	*Fagus sylvatica*	loess	0.7121-0.7136	0.7090	71-79%[2]
		Fagus sylvatica	shales/siltstones	0.7162-0.7176	0.7092	72-82%[2]
Bélanger and Holmden	Saskatchewan, Canada	*Pure black spruce stand*	granite	0.7220-0.7471	0.7145	20-30%
		Mixedwood: spruce, aspen and pine				40-75%
Miller et al. (1993)	New York, USA	*Picea rubens, Abies balsamifera and Betula alleghaniensis*	anorthosite	0.7052-0.7066	0.7093	53%[3]
Vitousek et al. (1999)	Hawaii	*Metrosideros polymorpha*	basalt (wettest sites)	0.7035	0.7092	~30%[3]
		Metrosideros polymorpha	basalt (dryess sites)	0.7035	0.7092	<20%[3]
Bailey et al. (1996)	New Hampshire, USA	*Picea rubens , Acer saccharum* and *Fagus grandifolia*	metapelite	0.7251	0.7100	32%[3]
Blum et al. (2002)	New Hampshire	*Picea rubens, Abies balsamifera*	metasedimentary with	0.7216	0.7106	5%
		Fagus grandifolia, Betula alleghaniensis	granitoid and mafic dykes	0.7216	0.7106	20-25%
		Acer saccharum		0.7216	0.7106	40%
Bern et al. (2005)	Costa Rica	*Brosimum utile , Schizolobium parahyba*	basalt	0.7035-0.7039	0.7088	<10%[3]

[1] for 5 of 8 individuals

[2] variability is due to the selected Sr/Ca of the soil mineral weathering end-member

[3] calculations for Sr only

Table 2.

	Horizon	Sand+Silt	Clay[Ψ]	pH[£]	Exch. Ca[§]	ECEC[t]
		%		H_2O	($cmol_c$ kg^{-1})	
Toposequence 1						
High (plot 1.1)	Forest floor	–	–	3.83	4.79	14.6
	Upper B	91.8	8.2	5.73	0.12	0.52
	Lower B	88.7	11.3	5.82	0.07	0.30
	C	90.0	10.0	5.46	0.14	0.53
Mid (plot 1.2)	Forest floor	–	–	3.95	25.7	38.4
	Upper B	88.9	11.1	5.50	0.47	1.26
	Lower B	84.0	16.0	5.01	0.57	1.36
	C	84.1	15.9	5.21	1.33	2.28
Bottom (plot 1.3)	Forest floor	–	–	4.52	36.2	46.6
	Upper B	59.8	40.2	4.64	6.71	14.5
	Lower B	58.7	41.3	6.31	6.03	11.3
	C	30.3	69.7	7.12	11.7	23.2
Toposequence 2						
High (plot 2.1)	Forest floor	–	–	4.21	29.4	37.6
	Upper B	80.9	19.1	5.51	6.12	11.0
	Lower B	77.2	22.8	5.62	7.30	13.7
	C	71.5	28.5	5.45	6.65	12.2
Mid (plot 2.2)	Forest floor	–	–	3.95	9.05	20.7
	Upper B	86.6	13.4	5.27	0.82	1.76
	Lower B	84.0	16.0	5.04	1.23	2.73
	R	–	–	–	–	–
Bottom (plot 2.3)	Forest floor	–	–	4.80	44.8	56.2
	Upper B	72.6	27.4	5.98	6.54	10.9
	Lower B	62.5	37.5	6.97	7.39	13.0
	C	36.8	63.2	6.88	11.4	20.6

[Ψ]Particle size distribution was determined on samples collected from the soil pit using the Horiba Partica LA-950 particle size laser analyzer; [£]Mineral soil pH was determined using a ratio of sample to water (distilled) of 1:2. A ratio of 1:5 was used for the forest floor to ensure proper wetting of the material; [§]Soil exchangeable cations were extracted using an unbuffered 0.1 mol l^{-1} $BaCl_2$ solution (Hendershot et al. 2007) and determined by atomic absorption or emission; [t]Effective cation exchange capacity (ECEC) was defined as Σ of Ca^{2+}, Mg^{2+}, K^+, Na^+, Fe^{2+}, Al^{3+}, and Mn^{3+}; H^+ was not included in the calculation of ECEC.

Table 3.

	Wood	Bark	Branches	Foliage
		g kg^{-1}		
Black spruce - Weetman and Weber (1972)	1.46 (1.44±0.40)	4.40	3.98	8.82 (8.94±3.26)
Jack pine - Weetman and Weber (1972)	0.75 (1.02±0.24)	4.32	2.22	3.06 (5.52±1.78)
Trembling aspen - Alban et al. (1978)	1.44 (2.44±0.73)	15.8	13.0	10.3 (13.9±1.40)
White spruce - Kimmins et al. (1985)	0.74 (1.00)	9.00	6.27	14.7 (12.9)

Table 4.

Sample Description	$^{87}Sr/^{86}Sr$	Sr (ppm)	Ca (ppm)	Sr/Ca (mmol/mol)
Precipitation				
Wet-only (*n* = 5)	0.71430	0.0024	0.270	4.36
Bulk deposition (*n* = 3)	0.71498	0.0034	0.379	3.70
Snow (*n* = 4)	0.71770	0.0008	0.380	1.38
snow (30%) and bulk deposition (70%)	0.71556	0.0023	0.341	3.24
Toposequence 1				
High (plot 1.1)				
Foliage				
jack pine	0.71529	38.9	6285	2.83
trembling aspen	0.71793	89.8	12703	3.23
black spruce (young)	0.71888	46.0	6254	3.36
black spruce (old)	0.71541	67.7	10071	3.07
Stemwood				
jack pine	0.71408	6.43	1268	2.32
trembling aspen	0.71551	33.8	3274	4.73
black spruce (old)	0.71546	11.1	1761	2.89
Soil solutions				
forest floor, 10 cm	0.71459	0.0314	6.40	2.24
upper B horizon, 35 cm	0.71062	——	——	——
Extracts (lower B horizon, 50-75 cm)				
$BaCl_2$	0.71434	2.99	41.1	33.3
1N HNO_3 (whole soil)	0.71552	1.47	314	2.14
1N HNO_3 (fine sand only)	0.73231	——	——	——
1N HNO_3 (silt and clay only)	0.72567	——	——	——
concentrated HNO_3	0.73935	2.65	629	1.93
Residue	0.70742	——	——	——
Mid (plot 1.2)				
Foliage				
jack pine	0.71670	11.0	6794	0.74
trembling aspen	0.72100	128	15443	3.78
black spruce (young)	0.71967	31.7	7742	1.88
black spruce (old)	0.72159	14.5	3748	1.77
Stemwood				
jack pine	0.71773	3.91	1001	1.79
trembling aspen	0.71690	21.9	1915	5.24
black spruce (old)	0.72086	7.34	1894	1.77
Soil solutions				
forest floor, 10 cm	0.72239	0.0980	16.6	2.70
upper B horizon, 35 cm	0.71891	0.0632	6.23	4.64
Extracts (lower B horizon, 50-75 cm)				
$BaCl_2$	0.71115	3.95	117	15.5
1N HNO_3	0.73274	1.59	604	1.20
concentrated HNO_3	0.74966	3.70	829	2.04
residue	0.70697	——	——	——
Low (plot 1.3)				
Foliage				
trembling aspen	0.72599	90.8	13612	3.05
black spruce (young)	0.72994	51.2	6050	3.87
black spruce (old)	0.72499	56.5	11030	2.34
white spruce	0.72218	125	12911	4.41
balsam poplar (outside plot)	0.72181	89.6	13684	3.00
Stemwood				
trembling aspen	0.72861	11.3	2120	2.43
black spruce (old)	0.72967	38.3	1658	10.6
white spruce	0.72189	9.39	995	4.32
balsam poplar	0.72146	28.0	4987	2.57
Soil solutions				
forest floor, 10 cm	0.72984	0.0448	7.46	2.75
upper B_1 horizon, 22 cm	0.72922	0.0602	7.58	3.63
upper B_2 horizon, 35 cm	0.73248	0.0736	10.2	3.29
Groundwater				
1.4 m	0.73025	0.104	13.2	3.62
1.8 m	0.73140	0.169	27.5	2.81
Extracts (lower B horizon, 50-75 cm)				
$BaCl_2$	0.73544	23.4	2393	4.47
1N HNO_3	0.74713	8.92	1233	3.31
concentrated HNO_3	0.77743	10.4	1455	3.28
residue	0.72397	——	——	——

Table 4. (continued)

Sample Description	$^{87}Sr/^{86}Sr$	Sr (ppm)	Ca (ppm)	Ca/Sr (mol/mol)
Toposequence 2				
High (plot 2.1)				
Foliage				
black spruce - a	0.71907	81.0	16756	2.21
black spruce - b	0.71813	65.4	9471	3.16
jack pine	0.71795	11.1	3487	1.46
Stemwood				
black spruce - b	0.71682	13.8	924	6.82
jack pine	0.71890	3.46	782	2.02
Soil solutions				
forest floor, 10 cm	0.71788	0.0373	7.71	2.21
upper B horizon, 35 cm	0.72770	0.0513	6.55	3.58
Extracts (lower B horizon)				
$BaCl_2$	0.72244	14.9	1445	4.73
1N HNO_3	0.73697	4.33	713	2.78
concentrated HNO_3	0.79432	12.5	1521	3.77
residue	0.71763	——	——	——
Mid (plot 2.2)				
Foliage				
black spruce - a	0.72976	27.6	7883	1.60
black spruce - b	0.72748	18.7	7841	1.09
Stemwood				
black spruce - b	0.72816	7.22	1020	3.24
Soil solutions				
forest floor, 10 cm	0.72208	0.0310	3.59	3.95
upper B horizon, 35 cm	0.72437	0.0344	2.80	5.63
Extracts (lower B horizon)				
$BaCl_2$	0.71466	5.38	231	10.6
1N HNO_3	0.73629	2.46	903	1.25
concentrated HNO_3	0.82285	4.60	1107	1.90
residue	0.71222	——	——	——
Low (plot 2.3)				
Foliage				
black spruce - a	0.72790	48.3	10071	2.19
black spruce - b	0.72919	47.6	10355	2.10
Stemwood				
black spruce - b	0.72926	9.74	1356	3.29
Soil solutions				
forest floor	0.72903	0.0411	5.63	3.34
upper B_1 horizon, 22 cm	0.72710	0.0447	6.03	3.39
upper B_2 horizon, 35 cm	0.73017	0.0422	5.90	3.28
Groundwater				
1.4 m	0.72576	0.0542	8.39	2.96
1.8 m	0.72939	0.114	17.1	3.04
Extracts (lower B horizon, 50-75 cm)				
$BaCl_2$	0.72970	11.4	1234	4.21
1N HNO_3	0.73924	4.20	1159	1.66
concentrated HNO_3	0.77304	13.2	1909	3.16
residue	0.71496	——	——	——
Streamwater (*n* = 8)	0.72126	0.0366	4.86	3.44
Granite				
Bulk	0.70893	467	19022	5.63
1 N HNO_3 Leach	0.71516	——	——	——
15 N HNO_3 Leach	0.89504	——	——	——
Corrected for ^{87}Sr growth (Rb = 43 ppm)	0.70676	——	——	——

Table 5.

	SiO_2	Al_2O_3	Fe_2O_3	MnO	MgO	CaO	Na_2O	K_2O	P_2O_5
	%								
Toposequence 1									
High (plot 1.1)	73.2	14.3	2.61	0.04	1.05	2.80	4.19	1.71	0.09
Mid (plot 1.2)	73.6	14.2	2.29	0.04	0.95	2.73	4.30	1.71	0.08
Bottom (plot 1.3)	65.5	17.3	6.34	0.08	2.79	1.93	2.22	3.17	0.16
Toposequence 2									
High (plot 2.1)	67.7	16.2	5.31	0.07	2.29	2.44	2.91	2.67	0.12
Mid (plot 2.2)	70.4	14.7	3.80	0.06	1.90	2.93	3.48	2.45	0.12
Bottom (plot 2.3)	67.8	15.4	4.91	0.09	2.30	2.88	3.03	2.62	0.19
Granite	71.3	16.1	1.93	0.03	0.71	2.58	5.15	1.90	0.07

Total iron present has been recalculated as Fe_2O_3.

Table 6.

	Toposequence 1			Toposequence 2		
	Plot 1.1 (high)	Plot 1.2 (mid)	Plot 1.3 (low)	Plot 2.1 (high)	Plot 2.2 (mid)	Plot 2.3 (low)
$^{87}Sr/^{86}Sr$ weathering end-member						
1 N HNO_3	0.726	0.733	0.747	0.737	0.736	0.739
15 N HNO_4	0.739	0.750	0.777	0.794	0.823	0.773
$^{87}Sr/^{86}Sr$ in mixture						
Trees	0.716	0.720	0.725	0.718	0.728	0.729
Forest floor pools	0.715	0.722	0.730	0.718	0.722	0.729
Mole fraction of Ca from atmospheric sources[2,3]						
Vegetation pools						
1 N HNO_3 weathering end-membe	0.94	0.70	0.63	0.84	0.31	0.37
15 N HNO_3 weathering end-mem	0.98	0.86	0.82	0.96	0.86	0.74
Average	0.96	0.78	0.73	0.90	0.59	0.55
Soil pools (FF)						
1 N HNO_3 weathering end-membe	IND	0.53	0.47	0.86	0.62	0.36
15 N HNO_3 weathering end-mem	IND	0.77	0.74	0.97	0.93	0.73
Average	IND	0.65	0.60	0.91	0.77	0.55
Grand average (vegetation and so	0.96	0.72	0.66	0.91	0.68	0.55
% rsd (1σ)		13	13	1	20	1

1. The 1.0N HNO_3 leach of the silt to fine clay fraction was used in the mixing calculations.
2. Ca apportionment results were calculated using Equation 1 (see text) and data from Table 4: including, plot averages of $^{87}Sr/^{86}Sr$ and Sr/Ca data for trees, soil pools, and seasonally averaged atmospheric deposition.
3. The Ca apportionment results $(Ca_a/(Ca_a+Ca_w)_{veg}$ in Table 5 of Holmden and Bélanger (2010) were calculated from the modeled Ca fluxes and, thus, differ from those reported here which are based on Equation 1.

IND = Indeterminate. The mixing equation cannot be solved because the $^{87}Sr/^{86}Sr$ of the vegetation or soil pool is not bracketed by end-members to mixing.